SIMPLIFYING INDEFINITE FIBRATIONS ON 4–MANIFOLDS

R. İNANÇ BAYKUR AND OSAMU SAEKI

Abstract. The main goal of this article is to connect some recent perspectives in the study of 4–manifolds from the vantage point of singularity theory. We present explicit algorithms for simplifying the topology of various maps on 4–manifolds, which include broken Lefschetz fibrations and indefinite Morse 2–functions. The algorithms consist of sequences of moves, which modify indefinite fibrations in smooth 1–parameter families. These algorithms allow us to give purely topological and constructive proofs of the existence of simplified broken Lefschetz fibrations and Morse 2–functions on general 4–manifolds, and a theorem of Auroux–Donaldson–Katzarkov on the existence of certain broken Lefschetz pencils on near-symplectic 4–manifolds. We moreover establish a correspondence between broken Lefschetz fibrations and Gay–Kirby trisections of 4–manifolds, and show the existence and stable uniqueness of simplified trisections on all 4–manifolds. Building on this correspondence, we also provide several new constructions of trisections, including infinite families of genus–3 trisections with homotopy inequivalent total spaces, and exotic same genera trisections of 4–manifolds in the homeomorphism classes of complex rational surfaces.

Contents

1. Introduction

An *indefinite fibration* is a smooth map from a compact smooth oriented 4–manifold onto an orientable surface, with simplest types of stable and unstable singularities; its singular locus consists of indefinite folds and cusps along embedded circles (*round locus*), and Lefschetz singularities along a disjoint discrete set. Its fibers are smooth orientable surfaces and singular surfaces obtained by collapsing embedded loops on them. The class of indefinite fibrations[1] naturally includes *broken Lefschetz fibrations* (when there are no cusps) and *indefinite Morse 2– functions* (no Lefschetz singularities), both of which received a hefty amount of attention over the past decade; e.g. [2, 4, 5, 6, 7, 8, 9, 10, 13, 14, 24, 26, 27, 33, 34, 35, 37, 38, 42, 51, 55, 64, 65, 70, 71, 79, 80]. Moreover, a special class of generic maps, which are "almost" indefinite, except for a single definite fold circle, underline the recently emerging theory of *trisections* of 4–manifolds; e.g. [1, 12, 16, 17, 23, 28, 36, 43, 44, 49, 52, 53, 54, 58, 59, 60, 61, 67]; also see [50] and references therein.

The main objective of this paper is to bridge between these recent approaches in the study of 4–manifolds from the viewpoint of singularity theory. We provide explicit algorithms which immensely *simplify* the topology of indefinite fibrations, and employ them to present purely topological and constructive proofs of the existence of simplified broken Lefschetz fibrations, pencils, and trisections. As a biproduct, we obtain a rather surprising result: the existence of *simplified Gay–Kirby trisections* on all 4–manifolds (which appears for the first time in this work, with further examples featured in the sequel [12]), for which there is a stable uniqueness result as well.

Let us first review the technical background. Our algorithms consist of sequences of moves that modify indefinite fibrations in smooth 1–parameter families. We describe several procedures of this type, especially for maps onto the 2–sphere, to derive an indefinite fibration —roughly— with the property that *every fiber*

- is obtained from a fixed regular fiber, by fiberwise 2–handle attachments (*directed*),
- contains at most one fold or cusp point (*embedded* round image),
- is connected (*fiber-connected*),
- if regular, is either of genus g or $g-1$ (*simplified*),

and we achieve these properties cumulatively. Here, what makes an indefinite fibration "simpler" is in essence quantified by the complexity of the handle decomposition induced by the fibration; e.g. the second property allows one to describe the 4–manifold by *round 2–handle* (circle times a 2–handle) attachments to a simple handlebody for a Lefschetz fibration over the 2–disk, and the fourth makes it possible to do it with a single round 2–handle [6]; cf. [26]. Simplified fibrations induce decompositions of the 4–manifold into elementary fibered cobordisms between surface bundles over circles, suitable for calculating Floer theoretic invariants, such as Heegaard–Floer [62, 63, 45, 46, 47, 48], Lagrangian matching [64, 65], or quilted Floer invariants [75, 76].

Each homotopy move we use corresponds to a bifurcation in a smooth 1–parameter family of indefinite fibrations, which may involve a single point (*mono-germ move*) or two/three points (*multi-germ move*), and locally changes the topology of the fibers. Many of these moves have already been studied and employed by several authors, most notably, by Levine, Hatcher–Wagoner, Eliashberg–Mishachev, Lekili, Williams, Gay–Kirby, Behrens–Hayano, and the authors of this article [5, 6, 14, 27, 32, 55, 56, 70, 71, 79, 80]. As we review mono-germ and multi-germ moves, we will identify a list of *always-realizable base diagram moves*; namely,

[1]The name "indefinite fibrations" is indeed a mutual compromise for "indefinite generic maps" (indefinite Morse 2–functions) and "broken Lefschetz fibrations". Other authors used "wrinkled fibrations" [55] and "broken fibrations" [79] for the same class of maps, among others.

local modifications of the singular image on the base (largely corresponding to Reidemeister type moves for fold images), which can be always realized by a homotopy move for indefinite fibrations.

Our first main result is the following:

Theorem 1.1. *Let X be a closed oriented connected 4–manifold. There is an explicit algorithm consisting of sequences of always-realizable mono-germ and multi-germ moves, which homotopes any given indefinite fibration $f\colon X \to S^2$ to a simplified indefinite fibration $g\colon X \to S^2$, which is fiber-connected, directed, has embedded singular image and connected round locus. It suffices to use mono-germ moves flip, unsink, and cusp merge, and multi-germ moves push, criss-cross braiding, and Reidemeister type moves* $\mathrm{R2}^0$, $\mathrm{R2}^1$, $\mathrm{R2}_2$, $\mathrm{R3}_2$, $\mathrm{R3}_3$.

Theorem 1.1 will follow from slightly more general procedures, each to strike one of the four properties we listed earlier, where it will suffice to use even narrower selection of moves; see Theorems 4.1 and 4.2, Proposition 4.4.

There is a quantitative and a qualitative advantage to the homotopies we construct. The list of moves in the second part of the theorem comprises less than a fourth of all the elementary moves that naturally arise in bifurcations in generic homotopies of indefinite fibrations (and less than a half of those with only indefinite singularities), along with a special move: the criss-cross braiding move, which is a combination of homotopy moves that are not always-realizable themselves; see Proposition 3.3. In particular, the process does not involve introduction/elimination of a 1–dimensional round locus component, known as birth/death. On the other hand, our exclusive use of only always-realizable moves via base diagrams eliminates the need to carry around the very-hard-to-track information for justifying the validity of certain moves.

A necessary condition for an oriented embedded 1–manifold Z in a closed oriented 4–manifold X to be the round locus of an indefinite fibration is that Z is null-homologous, i.e. $[Z] = 0$ in $H_1(X;\mathbb{Z})$; see Proposition 5.1. Our second theorem shows that it is also a sufficient condition for realizing Z as the round locus of some indefinite fibration, after a homotopy:

Theorem 1.2. *Let X be a closed oriented connected 4–manifold and Z be a (non-empty) null-homologous closed oriented 1–dimensional submanifold of X. There is an explicit algorithm consisting of sequences of always-realizable mono-germ and multi-germ moves, which homotopes any given indefinite fibration $f\colon X \to S^2$ with non-empty round locus to a fiber-connected, directed broken Lefschetz fibration $g\colon X \to S^2$ with embedded singular image, whose round locus Z_g coincides with Z as oriented 1–manifolds. It suffices to use mono-germ moves flip, unsink, cusp merge, and multi-germ moves push, criss-cross braiding, and Reidemeister type moves* $\mathrm{R2}^0$, $\mathrm{R2}^1$, $\mathrm{R2}_2$, $\mathrm{R3}_2$, $\mathrm{R3}_3$.

There are two local models around an indefinite fold circle without cusps; yielding them to be marked as *untwisted* (even) or *twisted* (odd). Akin to the zero locus (the singular locus) of a near-symplectic form [66], the number of untwisted components of an indefinite fibration on a closed oriented 4–manifold X is congruent modulo 2 to $1 + b_1(X) + b_2^+(X)$; see Proposition 5.2. The full version of the above theorem, Theorem 5.3, will show that this necessary condition on the number of untwisted components is also sufficient; we can adjust our algorithm to realize Z as the round locus of an indefinite fibration with prescribed local models.

Broken Lefschetz fibrations and pencils were introduced by Auroux, Donaldson and Katzarkov in [4], where they proved that every near-symplectic 4–manifold admits a directed broken Lefschetz pencil with embedded round image using approximately holomorphic geometry. In [5], the first author of this article, using the work of the second author in [70], gave an elementary

proof of the existence of broken Lefschetz pencils on near-symplectic 4–manifolds via singularity theory, and also established that every closed oriented 4–manifold admits a broken Lefschetz fibration. A number of alternate proofs of these existence results and their improvements quickly followed: Building on Gay and Kirby's earlier work on *achiral* Lefschetz fibrations in [24] (where Lefschetz singularities with opposite orientation are allowed), which made extensive use of round 2–handles, the existence of broken Lefschetz fibrations with *directed, embedded round image* on every closed oriented 4–manifold was shown in [55, 7, 2]. An alternate singularity theory proof, backed by Cerf theory, was later given in [27] to obtain *fiber-connected* broken Lefschetz fibrations.

Despite this variety however, all the existence proofs so far either made use of geometric results which did not yield to explicit constructions, or fell short of producing broken Lefschetz fibrations/pencils with *simplified* topologies. Handlebody proofs made essential use of Eliashberg's classification of over-twisted contact structures [20] and Giroux's correspondence between open books and contact structures [29], making these procedures non-explicit. Singularity theory proofs came with rather explicit algorithms, but did not succeed in producing a *directed* indefinite fibration with *embedded* round locus. Moreover, none of these works could reproduce an important aspect of Auroux, Donaldson and Katzarkov's pencils: in [4], the authors were able to build their broken Lefschetz pencils so that the 1–dimensional round locus would coincide with the zero locus (singular locus) of the near-symplectic form.

By incorporating our new algorithms to simplify the topology of indefinite fibrations, we will improve on the singularity theory approach to derive purely topological and explicit constructions:

Theorem 1.3. *Let X be a closed oriented 4–manifold and Z be a (non-empty) null-homologous closed oriented 1–dimensional submanifold of X. Then, there exists a fiber-connected, directed broken Lefschetz fibration $f\colon X \to S^2$ with embedded round image, whose round locus Z_f matches Z. Given any generic map from X to S^2, such f can be derived from it by an explicit algorithm. If X admits a near-symplectic form ω with non-empty zero locus Z_ω, then there exists a fiber-connected directed broken Lefschetz pencil f on X with embedded round image, whose round locus Z_f matches Z_ω and $\omega([F]) > 0$ for any fiber F of f.*

We will prove the two parts of this theorem in stronger forms in Theorems 6.1 and 6.5, and Corollaries 6.2 and 6.6.

In the last section, we turn to trisections of 4–manifolds introduced by Gay and Kirby in [28], which are 4–dimensional analogues of Heegaard splittings of 3–manifolds. Just like how one can study Heegaard splittings as certain Morse functions, or as decompositions into two standard handlebodies along with boundary diffeomorphisms, or as Heegaard diagrams, trisections can be studied in three different ways: as certain generic maps (trisected Morse 2–functions), decompositions into three standard handlebodies along with pairwise partial boundary diffeomorphisms, and trisection diagrams [28]. Adopting the first perspective, we simply refer to a trisected Morse 2–function yielding a trisection decomposition as a *trisection*. This allows us to study trisections as "almost" indefinite fibrations, with special topology: they are generic maps to the disk, where a single definite fold circle along the boundary of the disk encloses the image of a fiber-connected, outward-directed indefinite generic map, that can be split into three slices (slicing the disk from a point in the innermost region) so that each sector contains g' fold arcs, $g' - k'$ of which contain a single cusp; see Figure 1. The preimages of these three slices are the three solid handlebodies $X_i \cong \natural^k(S^1 \times B^3)$ of the decomposition $X = X_1 \cup X_2 \cup X_3$.

We will provide various algorithmic constructions of trisections of 4–manifolds, based on our simplifications of generic maps through generic homotopy moves. Our main result establishes a correspondence between simplified broken Lefschetz fibrations and trisections:

Theorem 1.4. *Let X be a closed oriented connected 4–manifold. If there is a genus–g simplified broken Lefschetz fibration $f\colon X \to S^2$ with $k \geq 0$ Lefschetz singularities and $\ell \in \{0,1\}$ round locus components, then there is a simplified (g',k')–trisection of X, with $(g',k') = (2g+k-\ell+2, 2g-\ell)$. If X admits a simplified (g',k')–trisection, then there is a fiber-connected, directed broken Lefschetz fibration $f\colon X \to S^2$ with embedded round image, which has regular fibers of highest genus g and with k Lefschetz singularities, where $g = g'+2$ and $k = 3g' - 3k' + 4$.*

Here the genus of a simplified broken Lefschetz fibration is the genus of the highest genus regular fiber, and when $\ell = 0$, it is an honest Lefschetz fibration.

We will prove slightly stronger versions of both directions of the above theorem in Theorem 7.1 and Proposition 7.6. A by-product of our construction of trisections from simplified broken Lefschetz fibrations is the existence of *simplified trisections* on arbitrary 4–manifolds, which, combined with our algorithmic constructions of simplified broken Lefschetz fibrations, can be obtained from any given generic map; see Corollary 7.4. Simplified trisections constitute a subclass of the special Morse 2–functions yielding trisections, where for a simplified trisection, we in addition have embedded singular image ("no non-trivial Cerf boxes between sectors") and cusps only appear in triples on innermost circles; see Figure 42 and cf. [28]. Similar to simplified broken Lefschetz fibrations (versus arbitrary broken Lefschetz fibrations), simplified trisections are amenable to a characterization in terms of Dehn twist factorizations in mapping class groups of surfaces, and our algorithm can be translated to an algorithm that turns a handle decomposition for a simplified broken Lefschetz fibration to a *simplified trisection diagram* [36]. Importantly, Gay and Kirby's fundamental result on the stable uniqueness of trisection decompositions [28] holds within the subclass of simplified trisection *decompositions* as well. See Remarks 7.5 and 7.8. Note that the stable uniqueness result is for the *decompositions* one obtains from simplified trisection maps.

Finally, building on the above correspondence between simplified broken Lefschetz fibrations and trisections, we construct some interesting families of trisections. In Corollary 7.9, we show that there are infinitely many homotopy inequivalent 4–manifolds admitting (g',k')–trisections, for each $g' \geq 3$ and $g'-2 \geq k' \geq 1$. In contrast, any (g',k') trisection with $g' < 3$ or $g' \geq k' \geq g'-1$ is standard [60, 59]. Furthermore, we show that there are trisections on complex rational surfaces, the three standard sectors of which can be re-glued differently to produce infinitely many exotic smooth structures on them; see Corollary 7.12. Many more new constructions of simplified trisections, based on our work here, appear in the sequel [12].

Acknowledgments. The results in this article have been promised for a long while, and several parts were presented by the authors in 2012 Nagano Singularity Conference, 2012 Japan Topology Symposium, and 2013 Bonn Geometry and Topology of 4–manifolds Conferences. We cordially thank all our colleagues who gently kept pushing us to complete this project. The authors would like to thank David Gay for his valuable comments on simplified trisections, and to Victor Goryunov and Toru Ohmoto for their comments which led to Remark 3.1. The authors also thank the referee for many invaluable comments, which improved the presentation of the paper. The first author was partially supported by the NSF grants DMS-0906912, DMS-1510395 and DMS-2005327. The second author has been supported in part by JSPS KAKENHI grants JP23244008, JP23654028, JP15K13438, JP16K13754, JP16H03936, JP17H01090 and JP17H06128.

2. Preliminaries

Here we review the definitions and basic properties of generic maps to surfaces, broken Lefschetz fibrations and pencils, along with moves which modify them in smooth 1–parameter families. All the manifolds and maps are assumed to be smooth.

2.1. **Fold, cusp and Lefschetz singularities; indefinite fibrations.**

Let $f\colon X \to \Sigma$ be a smooth map between compact connected oriented manifolds of dimensions four and two. In the following, we assume that $f^{-1}(\partial\Sigma) = \partial X$ and f is a submersion on a neighborhood of ∂X. Let $y \in \operatorname{Int} X$ be a *singular point* of f, i.e. $\operatorname{rank} df_y < 2$. The map f is said to have a *fold singularity* at y if there are local coordinates around y and $f(y)$ in which the map is given by

$$(t, x_1, x_2, x_3) \mapsto (t, \pm x_1^2 \pm x_2^2 \pm x_3^2),$$

and a *cusp singularity* if the map is locally given by

$$(t, x_1, x_2, x_3) \mapsto (t, x_1^3 + t x_1 \pm x_2^2 \pm x_3^2).$$

A fold or a cusp point y is *definite* if coefficients of all quadratic terms in the corresponding local model are of the same sign, *indefinite* otherwise. Note that an indefinite cusp is always adjacent to indefinite fold arcs.

A special case of Thom's transversality implies that any smooth map from an $n \geq 2$ dimensional space to a surface can be approximated arbitrarily well by a map with only fold and cusp singularities [57, 73, 78]. Such $f\colon X \to \Sigma$ is called a *generic map* (or an *excellent map*, or –more recently– a *Morse 2–function*). The *singular locus* Z_f of f is assumed to be in $\operatorname{Int} X$ and it is a disjoint union of finitely many circles, which are composed of finitely many cusp points, and arcs and circles of fold singularities. We call f an *indefinite generic* map if all of its fold singularities are indefinite.

On the other hand, the map f is said to have a *Lefschetz singularity* at a point $y \in \operatorname{Int} X$ if there are orientation preserving local coordinates around y and $f(y)$ so that f conforms to the complex local model

$$(z_1, z_2) \mapsto z_1\, z_2.$$

A *broken Lefschetz fibration* is a surjective map $f\colon X \to \Sigma$ which is only singular along a disjoint union of finitely many Lefschetz critical points and indefinite fold circles. A *broken Lefschetz pencil* is then defined for $\Sigma = S^2$, when there is a non-empty, finite set B_f of *b*ase points in X, where f conforms to the complex local model

$$(z_1, z_2) \mapsto z_1/z_2,$$

and $f : X \setminus B_f \to S^2$ has only Lefschetz and indefinite fold singularities [4].

Since the set of generic maps is open and dense in an appropriate mapping space endowed with the Whitney C^∞ topology, every broken Lefschetz fibration can be approximated (and hence homotoped) to a map with only fold and cusp singularities. The works of the authors in [70] and in [5] showed that when the base $\Sigma = S^2$, one can effectively eliminate the definite fold singularities and cusps in order to homotope a generic map to a broken Lefschetz fibration, implying the abundance of broken Lefschetz fibrations. Moreover, as shown in [55], one can trade an indefinite cusp point with a Lefschetz singularity, and locally perturb a Lefschetz singularity into a simple indefinite singular circle with three cusp points, allowing one to switch between indefinite generic maps and broken Lefschetz fibrations in a rather standard way.

With these in mind, we call a smooth surjective map $f\colon X \to \Sigma$ an *indefinite fibration* if it is an indefinite generic map outside of a finite collection of Lefschetz singular points C_f. For

an indefinite fibration f, we will call the 1–dimensional singular locus Z_f the *round locus*, and its image $f(Z_f)$ the *round image* of f. Note that the restriction of an indefinite fibration to its round locus is an immersion except at the cusp points. Its round image is, generically, a collection of cusped immersed curves on Σ with transverse double points off the cusp points, which we will assume to be the case hereon. We can moreover assume that there is at most one Lefschetz singular point on any fiber, and also, Lefschetz critical values and round image are disjoint.

The *base diagram* of an indefinite fibration is the pair $(\Sigma, f(Z_f \cup C_f))$, where the image of any indefinite fold arc or circle is normally oriented by an arrow, which indicates the direction in which the topology of a fiber changes by a 2–handle attachment when crossing over the fold from one side to the other. This means that a generic fiber over the region the arrow starts, if connected, has one higher genus than the generic fiber over the region the arrow points into; hence the terminology, *higher* and *lower sides* [6].

For an indefinite fibration $f\colon X \to \Sigma$, we say that

- f is *outward-directed* (resp. *inward-directed*), if the round image of f is contained in a 2–disk D in Σ such that the complement of a regular value $z_0 \in D$ can be non-singularly foliated by arcs oriented from z_0 to ∂D, which intersect the image of each fold arc transversely in its normal direction (resp. the opposite direction),
- f has *embedded round image*, if f is injective on its round locus,
- f is *fiber-connected*, if every fiber $f^{-1}(z)$, $z \in \Sigma$, is connected.

We simply say f is *directed* if it is either outward or inward-directed; when $\Sigma = S^2$, one clearly implies the other.

All these properties are essentially about the round locus and not about Lefschetz critical points. Importantly, the topology of an indefinite fibration is much simplified when f satisfies these additional properties. In particular, any fiber-connected $f\colon X \to S^2$ with embedded round image and connected round locus (which implies directed), with all Lefschetz singularities on the higher side, can be captured by simple combinatorial data: an ordered tuple of loops on the highest genera generic fiber (say, the one over z_0) [6, 79]. Such $f\colon X \to S^2$ is said to be *simplified*.

2.2. **Near-symplectic structures.**

A closed 2–form ω on an oriented 4–manifold X is said to be *near-symplectic*, if at each point $x \in X$, either $\omega_x^2 > 0$ (non-degenerate), or $\omega_x = 0$ and the intrinsic gradient $\nabla\omega\colon T_xX \to \Lambda^2(T^*X)$ as a linear map has rank 3. The *zero locus* of ω, i.e. the set of points $x \in X$ where $\omega = 0$, is a 1–dimensional embedded submanifold of X denoted by Z_ω.

Take $\mathbb{R}^4$ with coordinates (t, x_1, x_2, x_3) and consider the 2–form

$$\Omega = dt \wedge dQ + *\,(dt \wedge dQ),$$

where $Q(x_1, x_2, x_3) = x_1^2 + x_2^2 - x_3^2$ and $*$ is the standard Hodge star operator on $\Lambda^2\mathbb{R}^4$. Define two orientation preserving affine automorphisms $\sigma_\pm$ of $\mathbb{R}^4$ by

$$\begin{aligned} \sigma_+(t, x_1, x_2, x_3) &= (t + 2\pi, x_1, x_2, x_3) \quad \text{and} \\ \sigma_-(t, x_1, x_2, x_3) &= (t + 2\pi, -x_1, x_2, -x_3). \end{aligned}$$

Restrict Ω to the product of $\mathbb{R}$ and the unit 3–ball D^3. Each $\sigma_\pm$ preserves Ω and the map $(t, x_1, x_2, x_3) \mapsto (t, Q(x_1, x_2, x_3))$, and thus, induces a near-symplectic form $\omega_\pm$ and an indefinite fold map $f_\pm$ on the quotient space $N_\pm = (\mathbb{R} \times D^3)/\sigma_\pm$. As shown in [41], any near-symplectic form ω around any component of Z_ω is locally (Lipschitz) equivalent to one of the two local near-symplectic models $(N_\pm, \omega_\pm)$. The circles in Z_ω which admit

neighborhoods (N_+, ω_+) are called *untwisted* or of *even* type, and the others *twisted* or of *odd* type. Similarly, each component of the round locus of a broken Lefschetz fibration/pencil f is locally equivalent to $(N_\pm, f_\pm)$, yielding the same terminology [6, 4]. Labeling the untwisted components with 0 and the twisted ones by 1, we obtain the *twisting data* for Z_ω or Z_f.

A 4–manifold X admits a near-symplectic structure X if and only if $b^+(X) > 0$ [40, 4]. (So near-symplectic 4–manifolds constitute a much larger class than the symplectic ones.) In [4], using approximately holomorphic techniques of Donaldson, the authors proved that for a given near-symplectic form ω on X, there is a directed broken Lefschetz pencil f with embedded round image, such that Z_f coincides with Z_ω with the same twisting data, and such that $\omega(F) > 0$ for any fiber F of f. They moreover proved a converse to this result by a Thurston–Gompf construction: if f is a broken Lefschetz pencil on X and there is an $h \in H^2(X; \mathbb{R})$ that evaluates positively on every component of every fiber of f, then X admits a near-symplectic form ω, such that Z_ω coincides with the round locus Z_f.

2.3. **Trisections of 4–manifolds.**

A (g, k)–*trisection* decomposition, with $g \geq k$, of a closed oriented connected 4–manifold X is a decomposition $X = X_1 \cup X_2 \cup X_3$, such that: (i) there is a diffeomorphism $\phi_i \colon X_i \to Z_k$ for each $i = 1, 2, 3$, and (ii) $\phi_i(X_i \cap X_{i+1}) = Y^-_{k,g}$ and $\phi_i(X_i \cap X_{i-1}) = Y^+_{k,g}$ for each $i = 1, 2, 3$ (mod 3). Here $Z_k = \natural^k(S^1 \times B^3)$, $Y_k = \partial Z_k = \sharp^k(S^1 \times S^2)$, and $Y_k = Y^+_{k,g} \cup Y^-_{k,g}$ is the standard genus g Heegaard splitting of Y_k obtained by stabilizing the standard genus k Heegaard splitting $g - k$ times. Note that $X_1 \cap X_2 \cap X_3$ is a closed genus–g surface, and g is said to be the *genus of the trisection*.

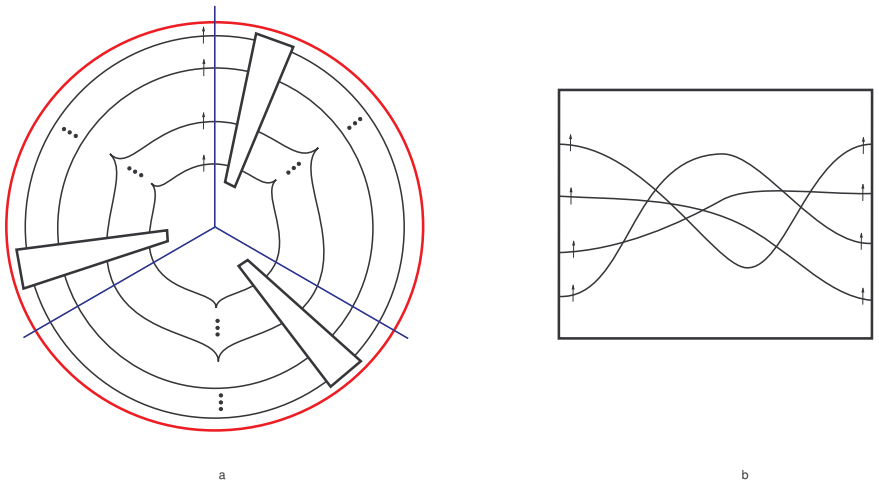

FIGURE 1. (a) Image of a generic map corresponding to a trisection: the outermost circle is the image of the definite fold circle, and in each box there is an arbitrary Cerf graphic in the sense of [28, §3]. The three half lines divide the image into three parts and their inverse images correspond to X_1, X_2 and X_3. (b) An example of a Cerf graphic.

Trisections of 4–manifolds are introduced by Gay and Kirby in [28]. They are to 4–manifolds, what Heegaard splittings are to 3–manifolds. Similar to how one can study Heegaard splittings in terms of certain Morse functions, trisections can be studied in terms of certain generic maps, called *trisected Morse* 2*–functions* in [28]. In this article, we will adopt this approach, and simply call any trisected Morse 2–function on X a *trisection* of X. This allows us to regard

trisections as "almost" indefinite directed generic maps. (Bearing in mind that many non-isotopic trisected Morse 2–functions can yield equivalent trisection decompositions.) Namely, in our language, a trisection corresponds to a generic map to the disk, with an embedded *definite* fold image enclosing the image of an outward-directed indefinite generic map, with a balanced distribution of cusps to three sectors as in Figure 1. The total numbers of indefinite fold arcs and indefinite fold arcs without cusps in each sector are g and k, respectively, where the arcs with cusps contain a single cusp. Note that the number of fold circles for this special kind of a generic map does *not* need to be equal to g, since raising/lowering them in the Cerf boxes, one may have a fold circle image wrapping around multiple times.

Remarkably, Gay and Kirby showed that just like the Reidemeister–Singer theorem for Heegaard splittings of 3–manifolds, trisections of 4–manifolds are unique up to *stabilization*, an operation which can also be described as an introduction of a nested triple of "wrinkles" [21] (or "eyes"); see [28].

3. Homotopies of indefinite fibrations and base diagram moves

In this section, we will discuss certain smooth 1–parameter families of indefinite fibrations, each of which amounts to a "move" from the initial fibration to the final one in the family. Many of these homotopy moves have been studied in varying levels of details by Levine, Hatcher–Wagoner, Eliashberg–Mishachev, Lekili, Williams, Gay–Kirby, Behrens–Hayano, and the authors of this article in [5, 6, 14, 27, 32, 55, 56, 70, 71, 79, 80]. Our goal here is to compile a comprehensive list of moves (with standardized terminology and notation) we can utilize in the rest of the article, for which we will refer to complete arguments in the existing literature, or provide them if needed. At the end of the section, we will add some *combination* moves to this list, which will play a key role in our topological modifications.

As we are largely interested in moves that will change the general topology of the fibration, we will often capture them by studying their singular image. A *base diagram move* is a transition from $(\Sigma, f_0(Z_{f_0} \cup C_{f_0}))$ to $(\Sigma, f_1(Z_{f_1} \cup C_{f_1}))$ realized by a smooth 1–parameter family $f_t : X \to \Sigma$, $t \in [0,1]$, such that f_t is an indefinite fibration for each t except for finitely many values in $(0,1)$. (Recall that we assume indefinite fibrations are also injective on their singular locus except possibly at fold double points.) Such a transition essentially happens locally around one point on Σ; however, the modification of the map f_t may occur around one, two, or three points in the domain X. Following singularity theory conventions, we will call it a *mono-germ move* if the move concerns a single point in X, and a *multi-germ move* otherwise.

We will often focus on only parts of the base diagram. Any Lefschetz critical value will be marked by a small cross sign in these diagrams. Figure 2 shows two examples. The *unsink* move of [55], which trades an indefinite cusp to a Lefschetz critical point, is a mono-germ move. It clearly changes the singular locus and the base diagram, though the isotopy type of the round locus stays the same. The *push* move of [6], which drags the Lefschetz critical point until its image is on the opposite side of the arrow of the round image, is a multi-germ move. In this case, the base diagram changes, but the isotopy type of the singular set does not.

Both of these are examples of base diagram moves that are *always-realizable* [55, 6]. That is, given a local configuration of a base diagram as on the left hand side of Figure 2, we can always find a 1–parameter family of smooth maps that realizes the relevant base diagram move. On the other hand, the *pseudo-inverses* of these two moves, *sink* and *pull* moves in Figure 2, are not always-realizable. A necessary and sufficient condition for a sink move is given in terms of vanishing cycles in [55]. A pull move can be realized if and only if the

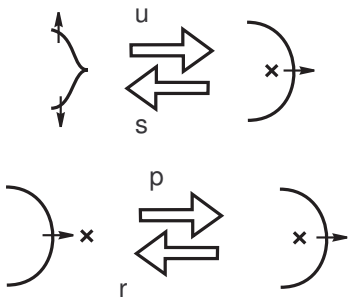

FIGURE 2. Unsink/sink and push/pull moves.

vanishing cycle for the Lefschetz critical point (on a reference fiber on the higher side) and that for the round locus can be chosen to be disjoint.

When there are additional conditions for a move to be realized, we indicate it by an exclamation mark; see e.g. the pseudo-inverses in Figure 2. Otherwise, the move is understood to be always-realizable. Importantly, *we will only use always-realizable base diagram moves* (some of which will be a combination of simpler moves) in this paper. Note that using unsink and push moves, we can always trade an indefinite cusp to a Lefschetz critical point, and we can push a Lefschetz critical value across any round image whose arrow is pointing towards it. Thus, we will not bother with cusps or Lefschetz critical points in such local diagrams. With this in mind, the collection of moves we cover in the next two subsections can be seen to be sufficient to pass from any given indefinite fibration to another (up to isotopy) by [79], as we also include Reidemeister type moves that can appear in bifurcations.

Remark 3.1. In fact, unsink and sink moves are closely related to the D_5–singularity of planar caustics, or the so called $I_{2,3}$–singularity of a map germ $(\mathbb{R}^2,0)\to(\mathbb{R}^2,0)$. A move similar to the unsink and sink moves appears as a special 1–dimensional section in a versal deformation of the D_5–singularity, see [74] and [81, Fig. 14].

3.1. **Mono-germ moves for indefinite fibrations.**

Figure 3 depicts several well-known mono-germ moves, which appear in generic homotopies, and are studied in detail in [56, 32, 21, 55, 79, 27, 14].

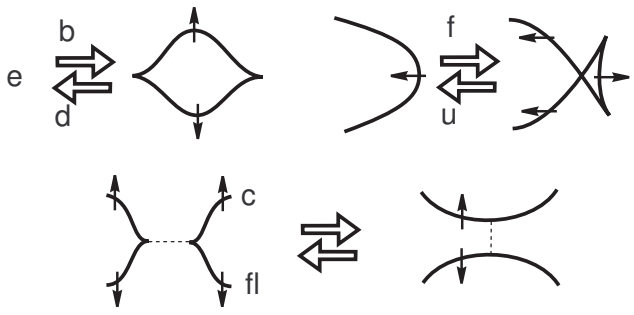

FIGURE 3. Classical mono-germ moves.

Note that *birth, death, flip* and *unflip* moves are always-realizable. For birth and flip moves, see, e.g. [68, Lemmas 3.1 and 3.3]. For death and unflip moves, [27, Lemmas 4.7

and 4.8] guarantee that they are realizable under certain conditions. As there are no other singularities appearing in the local pictures, these conditions are automatically satisfied in our case. A cusp merge can be performed if and only if there exists a joining curve connecting the pair of cusps used to eliminate them whose image is depicted by a dotted line in the diagram; in particular, this move is always-realizable when the fibers over the given local disk are connected. A necessary and sufficient condition for a fold merge is that the relevant vanishing cycles intersect transversely at one point on a reference fiber over the middle region [55, 79, 14]: in other words, if we take a vertical oriented line segment in the base depicted in the lower right of Figure 3, then its inverse image corresponds to a canceling pair of 1– and 2–handles (see also [27, Lemma 4.6]).

Figure 4 shows another example of a mono-germ move from [55] we denote by W, called *wrinkling*, which comes from the local perturbation of a Lefschetz critical point. (Here the pseudo-inverse W^{-1} may produce a Lefschetz type critical point with the wrong orientation, called an "achiral Lefschetz critical point".)

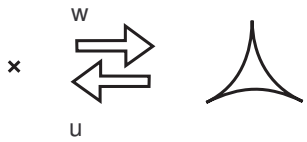

FIGURE 4. Wrinkling move.

Observe that all these moves, except for flip and unflip, change the set of the singular locus: a birth creates a new circle, a cusp merge corresponds to a "band move" for the set of singular points, etc. Flip and unflip moves, however, both preserve the isotopy type of the singular locus.

3.2. **Multi-germ moves and isotopies of the round locus.**

We now introduce several multi-germ moves, where the round locus simply goes through an isotopy, while the topology of the indefinite fibration changes, at times drastically. Many of these moves have already been studied in, e.g., [56, 32, 5, 24, 80, 35, 14]. Almost all of these multi-germ moves correspond to the well-known Reidemeister moves II and III for link diagrams in knot theory. However, base diagrams are not simple projections of 1–dimensional submanifolds, but they are the images of round loci under indefinite fibrations. Furthermore, each fold image has a normal orientation. Therefore, *there are multiple base diagram moves corresponding to a single Reidemeister type move* (even without any need to involve cusps or Lefschetz critical points in general, as we pointed out earlier) .

To have a uniform notation, Reidemeister II moves will be denoted by R2, decorated by subindices 0, 1 or 2, which indicate the number of fold arcs with normal arrows pointing into the bounded region, whereas their pseudo-inverses (which do not have any bounded regions) will be denoted by the same index in the superscript. Reidemeister III moves will be denoted by R3, decorated by subindices 0, 1, 2 or 3, which again indicate the number of fold arcs with normal arrows pointing into the bounded region. Note that the pseudo-inverse of an $\mathrm{R3}_i$ move is an $\mathrm{R3}_j$ move with $i + j = 3$; see Figures 5 and 6.

Base diagram moves of Reidemeister II type are depicted in Figure 5, where only one of each pair is always-realizable. For example, for the $\mathrm{R2}_0$ move, the diagram on the left hand side corresponds, in upward vertical direction, to a surface cross interval with a 2–handle and a 1–handle attached in this order. Horizontally, from left to right, the same diagram

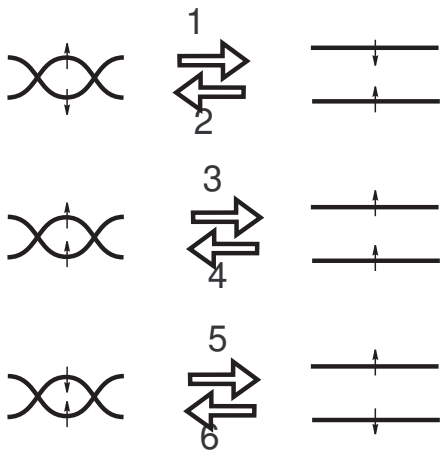

FIGURE 5. Reidemeister II type multi-germ moves.

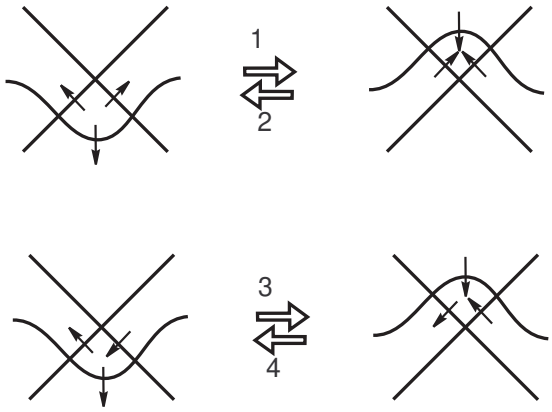

FIGURE 6. Reidemeister III type multi-germ moves.

corresponds to the following: first, the order of the two handle attachments is switched, then the 2–handle slides over the 1–handle, and finally the order is switched again. So, the $R2_0$ move is realized if and only if the handle-slide trace of the attaching circle of the 2–handle core can be isotoped away from the co-core of the 1–handle. On the other hand, the diagram on the right corresponds to a handle-slide in which the 1–handle slides over the 2–handle. The trace of the attaching region of a 1–handle can always be isotoped away from a 2–handle, so the move $R2^0$, the *pseudo-inverse* of $R2_0$, is always-realizable. Similar index arguments show that the moves $R2^1$ and $R2_2$ (applied to the middle part in this case) are always-realizable. For example, for the $R2_2$ move, the diagram on the left hand side corresponds to the following: first, the order of the two handle attachments is switched, then the 1–handle slides over the 2–handle, and finally the order is switched again. As the trace of the isotopy of the attaching 0–sphere of the 1–handle can be isotoped away from the co-core of the 2–handle, we can arrange it so that the handle slides take place completely away from the 2–handle. Therefore, the handle switches are not necessary, and consequently the $R2_2$ move is realized. On the other hand, the moves $R2_1$ and $R2^2$ are not realizable. (For the $R2_1$ move, see Remark 3.5.

The move $R2^2$ is not realizable if the attaching circle of the upper 2–handle winds along the lower 1–handle algebraically non-trivially, for example.)

As to base diagram moves of Reidemeister III type, we have those as depicted in Figure 6. We can prove that the move $R3_3$ is always-realizable by an argument similar to that for the move $R2_2$ above. Then, as shown in Figure 7, the move $R3_2$ is realized as a composition of always-realizable moves $R2^0$, $R3_3$ and $R2_2$. So $R3_2$ move is also always-realizable. For $R3_0$ and $R3_1$ moves, there are necessary conditions; cf. [80].

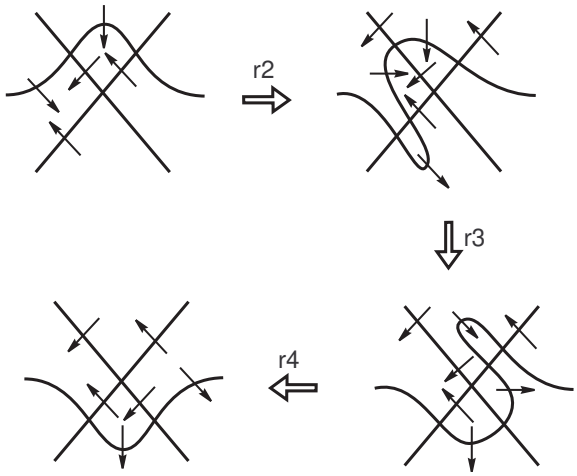

FIGURE 7. Realizing the $R3_2$ move.

Lastly, as multi-germ moves involving cusps, we have the *cusp–fold crossing* C–move and its pseudo-inverse, depicted in Figure 8. The C–move is always-realizable as seen by an argument in the cusp elimination technique of [56]; see also [80, Proposition 2.7]. The pseudo-inverse move C^{-1} is not always-realizable, for reasons similar to the case of $R2_0$ or $R2_1$.

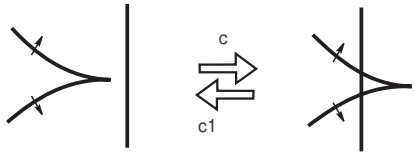

FIGURE 8. Passing a cusp through the round image and its pseudo-inverse. The normal orientation for the vertical round image component is irrelevant: both orientations are allowed.

3.3. **Some always-realizable combination moves.**

A combination homotopy move for an indefinite fibration consists of a sequence of mono-germ and multi-germ moves. Our first example is the *flip and slip move* of [5, Fig. 5], which can be used to turn an inward-directed circle in D inside out, so it becomes outward-directed. The flip and slip consists of a sequence of always-realizable mono-germ and multi-germ moves shown in Figure 9.

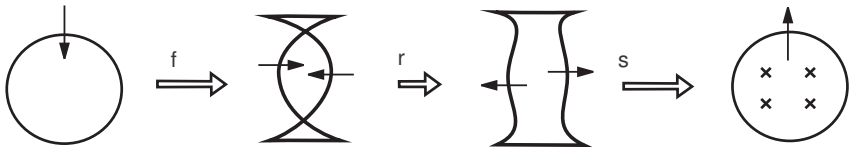

FIGURE 9. Flip and slip.

Another combination move we will introduce here consists of a sequence of not necessarily always-realizable moves, but the combined move itself is always-realizable as a whole, as follows.

Proposition 3.2. *Let D be a local disk containing the base diagram on the left hand side of Figure 10. Suppose that the fibers over the points in the region marked with $(*)$ are connected. Then, the* exchange move *depicted in Figure 10 is realizable. It is realized by a sequence of two flips, cusp merge,* $\mathrm{R3}_1$*, and unflip moves.*

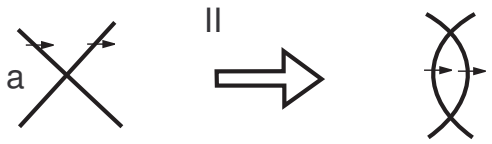

FIGURE 10. Exchange move

Proof. Let us identify the disk D with the square $I \times J$, where $I = J = [-1, 1]$, I corresponds to the vertical direction downward and J to the horizontal direction from right to left (see Figure 11). We regard $f^{-1}(D) = f^{-1}(I \times J)$ as a 1–parameter family of 3–manifolds $f^{-1}(\{t\} \times J)$, $t \in I$, which are obtained from $f^{-1}(\{t\} \times [-1, -1 + \varepsilon])$, $0 < \varepsilon << 1$, by attaching two 1–handles. By isotoping the handle slides that may possibly occur while $t \in I$ varies into intervals outside of I, we may assume that there occurs no handle slide for $t \in I$. Near $t = 0$, where the crossing of two fold arc images occurs, the crossing of two 1–handles occurs. Note that the 3–manifold $f^{-1}(\{t\} \times J)$ obtained by attaching the two 1–handles is connected for each t by our assumption.

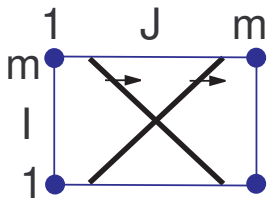

FIGURE 11. Identifying D with $I \times J$.

The exchange move can be decomposed into the the sequence of base diagram moves as depicted in Figure 12. The transition from (a) to (b) is realized by two flips. The transition from (b) to (c) is realized by a cusp merge, which is realizable as the relevant fibers are all connected by our assumption. The transition from (c) to (d) is realized by $\mathrm{R3}_1$ move, which

is not always-realizable. We will explain below why this transition is possible more in detail. Finally, the transition from (d) to (e) is realized by an unflip.

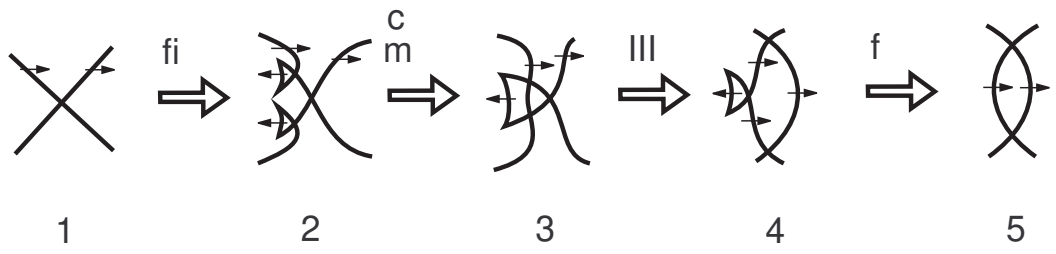

FIGURE 12. Base diagram moves for the exchange move.

It might be good to remind that here we are constructing a smooth 1–parameter family of maps (from a 4–manifold to a surface) which starts from a given indefinite fibration with a base diagram as in Figure 12 (a), and which ends up with a certain (not given!) indefinite fibration with a base diagram as in Figure 12 (e). That is, our goal is to show that we can appropriately choose indefinite fibrations with base diagrams as in Figure 12 (b)–(e); we are not trying to reconstruct *any* possible transition for such a sequence of base diagram moves. In particular, we can choose these maps so that the handle-slides are arranged as argued in the previous paragraphs.

Let us now show why the transition from (c) to (d) is possible. In order to see this, let us foliate the local disk in Figure 12 by horizontal sections (oriented from right to left, as $\{*\}\times J$) and consider the change in fiberwise handle attachments as we move from upper sections to lower ones "as we move the line segment". We focus on the transition from Figure 12 (c) to (d). For each local base diagram, a horizontal section corresponds to a surface cross interval with some handles attached (from right to left, as we find it more convenient to illustrate, using mostly 1–handles), and the vertical (downward) direction corresponds to a deformation of the handlebody. See Figure 13. For example, for each of the horizontal sections c_1 and d_1, we have two 1–handles h_1'' and h_1' attached in this order. Note that between any consecutive sections c_j, c_{j+1} or d_j, d_{j+1}, a birth–death or a crossing of critical values occurs. Note also that when we move down the line segment without passing through a birth–death or a crossing, some handle-slides may occur: more precisely, handles corresponding to critical values to the left may slide over those to the right.

Figure 14 describes Step (c) as follows. When the line segment passes through the upper cusp, a canceling pair of 1– and 2–handles (attached to the fiber in this order), say h_1 and h_2 (depicted in green in the figure), is created; see the picture for the horizontal section c_2. This canceling pair should be created on a sheet on which both h_1' and h_1'' have at least one of their attaching 2–disks. Then, we slide this pair of handles over the 1–handle h_1'. After switching the order of h_1 and h_1' as we pass the crossing, we slide h_1' and h_2 off h_1; see the picture for the horizontal section c_3. (Observe that a similar sequence of handle deformations take place as we move *upwards* from level c_6 to c_4.) Then, the 2–handle h_2 and the 1–handle h_1'' become a canceling pair.

Then, this sequence of moves can be deformed to that corresponding to Step (d) as depicted in Figure 15.

An intermediate step is as depicted in Figure 16, which shows that the transition from (c) to (d) is always realizable.

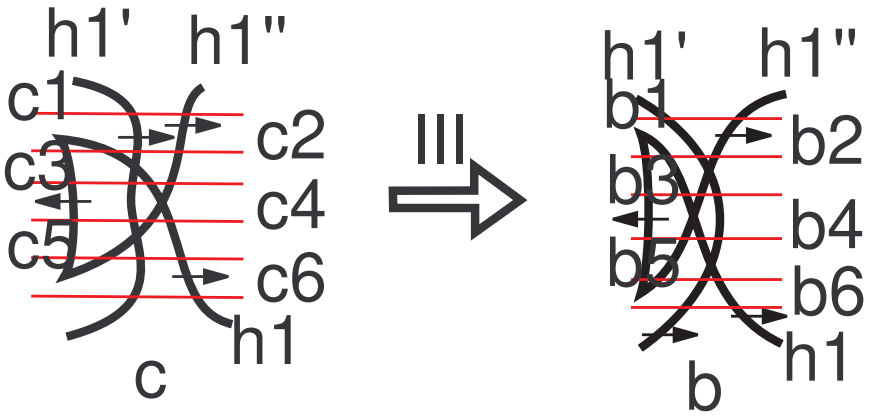

FIGURE 13. Six horizontal sections for (c) and (d) in Figure 12. Round image arcs with normal direction towards the right correspond to 1–handles h_1, h_1' and h_1''.

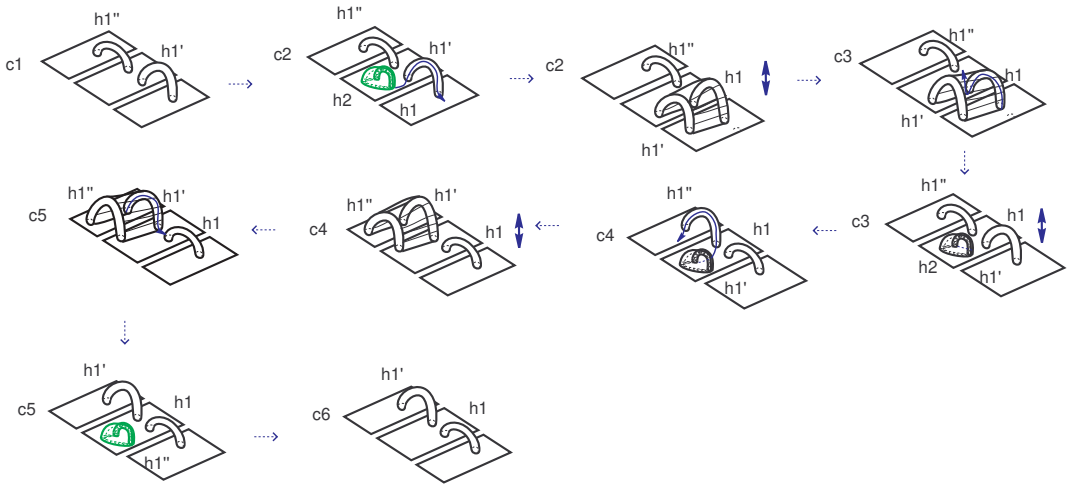

FIGURE 14. Step (c), where a cancelling pair of 1– and 2–handles appear, then the handle slides as above occur, and finally a cancelling pair vanishes.

This completes the proof of the proposition.

Let us give another argument based on singularity theory. We can construct a smooth map $F\colon V \to I\times J\times[0,1]$ of a compact 5–dimensional manifold with corners $V \cong f^{-1}(I\times J)\times[0,1]$ with the following properties.

(1) The map $F|_{F^{-1}(I\times J\times\{0\})}\colon F^{-1}(I\times J\times\{0\}) \to I\times J\times\{0\}$ coincides with
$$f|_{f^{-1}(I\times J)}\colon f^{-1}(I\times J) \to I\times J.$$
(2) The singular value set is as depicted in Figure 17.
(3) The map F restricted to $F^{-1}(\partial I\times J\times[0,1]) \cong f^{-1}(\partial I\times J)\times[0,1]$ coincides with the trivial 1–parameter family of maps
$$(f|_{f^{-1}(\partial I\times J)})\times \mathrm{id}_{[0,1]}\colon f^{-1}(\partial I\times J)\times[0,1] \to \partial I\times J\times[0,1].$$

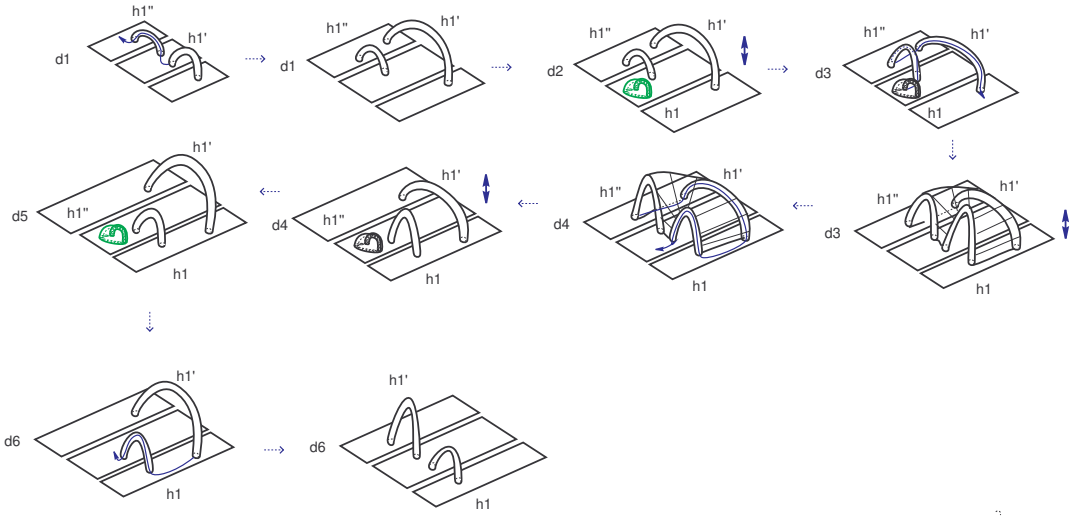

FIGURE 15. Step (d).

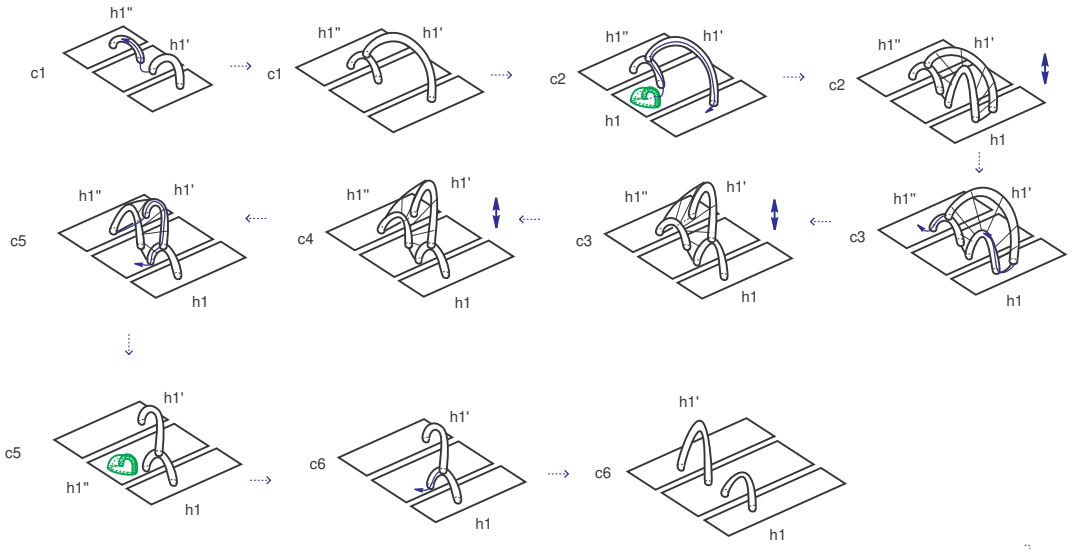

FIGURE 16. Intermediate step between Steps (c) and (d).

Note that F can be regarded as a homotopy of maps $f^{-1}(I \times J) \to I \times J$ parametrized by $[0,1]$, starting from $f|_{f^{-1}(I\times J)}$ and ending with an indefinite fibration whose base diagram is as depicted in the right hand side of Figure 10.

Such a smooth map F can be constructed, for example, as follows. As indicated in [32, Chapter V, §4], to a monkey saddle corresponds a 3–parameter family of functions on a connected 3–manifold, parametrized by a 3–ball. Then the map F corresponds to the southern hemisphere of the boundary of the parameterizing 3–ball for a monkey saddle on an appropriate 3–manifold. This argument directly proves that the exchange move is always realizable. □

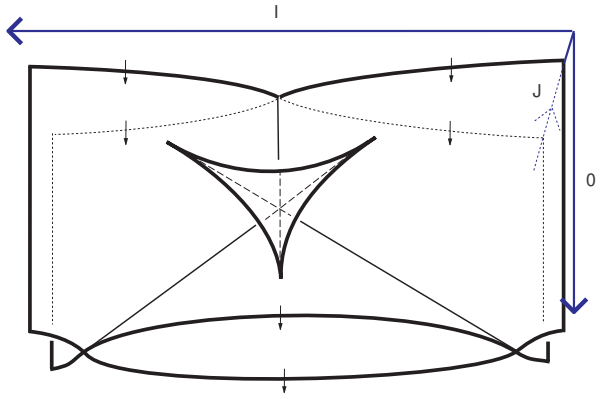

FIGURE 17. The singular value set of F in $I \times J \times [0,1]$.

Our next combination move is an immediate corollary of the above proposition:

Proposition 3.3 (Criss-cross braiding)**.** *Let D be a local disk containing the base diagram on the left hand side of Figure 18. Suppose that the fibers over the points in the region marked with $(*)$ are connected. Then, the criss-cross braiding depicted in Figure 18 is realizable. It is realized by a sequence of* $\mathrm{R2}^1$*, two flips, cusp merge,* $\mathrm{R3}_1$*, and unflip moves.*

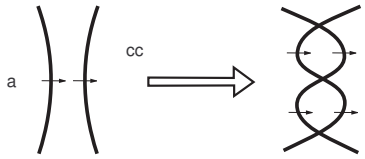

FIGURE 18. *Criss-cross braiding* that can be always-realized.

Proof. We first apply $\mathrm{R2}^1$ move. Then, by our assumption, we can apply Proposition 3.2 to one of the crossings to get the desired base diagram. □

Taking a closer look at our proofs of above propositions, we can identify some necessary conditions for the Reidemeister type moves we have not identified as always-realizable. We discuss these in the next several remarks.

Remark 3.4. In the proof of Proposition 3.2, we constructed a smooth map

$$F : V \to I \times J \times [0,1].$$

For $(s_1, s_2) \in I \times [0,1]$, set

$$F_{s_1,s_2} = p_J \circ F|_{F^{-1}(\{s_1\}\times J\times\{s_2\})} \colon F^{-1}(\{s_1\} \times J \times \{s_2\}) \to J,$$

where $p_J \colon I \times J \times [0,1] \to J$ is the projection to the second factor. This is a family of functions on a 3–manifold parametrized by $I \times [0,1]$. If $(s_1, s_2) \in \partial(I \times [0,1])$, then F_{s_1,s_2} has exactly two critical points of index 1. Observing the monkey saddle point carefully, we see that as $(s_1, s_2) \in \partial(I \times [0,1])$ varies, we have the handle slides as depicted in Figure 19.

Let us examine more carefully the handle slides involved in an exchange move. For this, let us investigate the homological behavior of the handle slides for the base diagrams on both sides of Figure 10. For $t_1 = -1 \in I$, let α (or β) denote the 1st homology class corresponding to

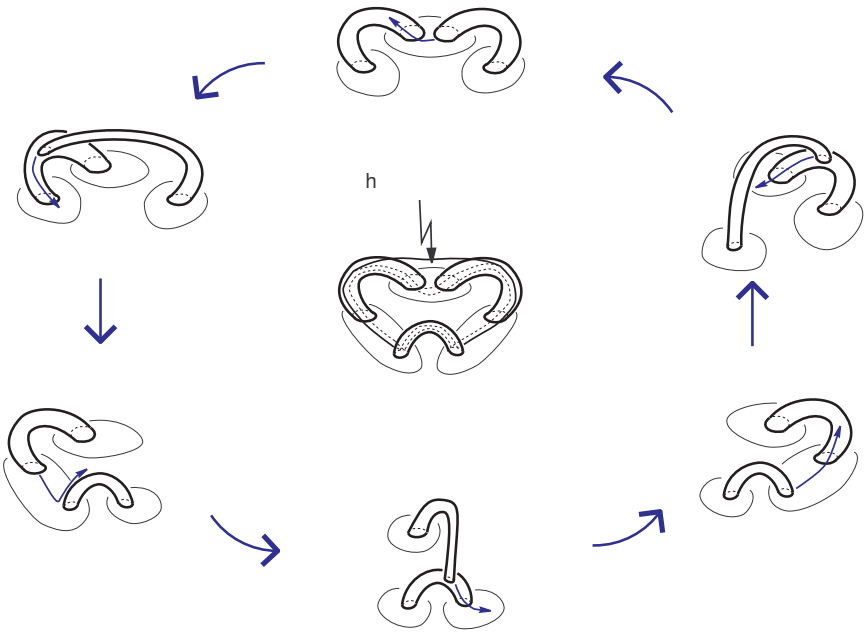

FIGURE 19. Handle slides for F_{s_1,s_2}, $(s_1,s_2) \in \partial(I \times [0,1])$. The central figure corresponds to $F_{0,1/2}$ which has exactly three critical points of index 1 with the same value, together with a critical point of index 2 over them.

the upper (resp. lower) 1–handle (see Figure 20). (Precisely speaking, we fix an orientation of each 1–handle, and then it represents an element of $H_1(f^{-1}(\{t_1\}\times J), f^{-1}(\{t_1\}\times\{-1\}); \mathbb{Z}) \cong \mathbb{Z}\oplus\mathbb{Z}$.) Let us first consider the base diagram on the left hand side of Figure 10. We consider the four parameter values of I indicated in Figure 20. We assume that for $t \in [t_1,t_2]$ (or $t \in [t_3,t_4]$), the upper 1–handle slides over the lower 1–handle homologically p times (resp. q times). We further assume that for $t \in [t_2,t_3]$ no handle slides occur. Then, a simple calculation shows that for the level $t_4 = 1 \in I$, the upper 1–handle represents the homology class $\beta + q(\alpha + p\beta) = q\alpha + (pq+1)\beta$, while the lower one represents $\alpha + p\beta$.

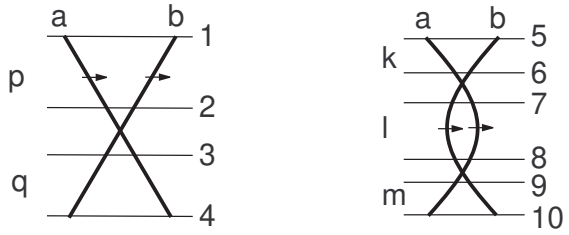

FIGURE 20. As $t \in I$ varies, the upper 1–handle slides over the lower one, and the corresponding homological "winding numbers" are denoted by p, q on the left hand side, while they are denoted by k, ℓ, m on the right hand side.

Let us play the same game for the base diagram on the right hand side of Figure 10. Then, using the notations indicated on the right hand side of Figure 20, we see that for the level $t_{10} =$

$1 \in I$, the upper 1-handle represents $\alpha+k\beta+m(\beta+\ell(\alpha+k\beta)) = (\ell m+1)\alpha+(k+m+k\ell m)\beta$, while the lower one represents $\beta + \ell(\alpha + k\beta) = \ell\alpha + (k\ell + 1)\beta$.

Therefore, if the transition between the both sides of Figure 20 is realized by homotopy, then we must have

$$\begin{aligned} q\alpha + (pq + 1)\beta &= \varepsilon_1((\ell m + 1)\alpha + (k + m + k\ell m)\beta), \\ \alpha + p\beta &= \varepsilon_2(\ell\alpha + (k\ell + 1)\beta) \end{aligned}$$

for some $\varepsilon_1, \varepsilon_2 \in \{-1, +1\}$. Here, note that ε_1 and/or ε_2 might be equal to -1, as the orientations of the 1–handles may be switched in the course of the handle slides. By a straightforward calculation, we see that these hold if and only if we have

$$\ell = \varepsilon_2,\ \varepsilon_1\varepsilon_2 = -1,\ p = k + \varepsilon_2,\ q = -m + \varepsilon_1.$$

In particular, we see that for $t \in [t_7, t_8]$ in the figure on the right hand side, the upper 1–handle must slide over the lower one homologically ± 1 time.

In the case of the proof of Proposition 3.2, we have $p = q = 0$, so $k = m = \varepsilon_1$ and $\ell = -\varepsilon_1$. This conforms to the proof of the lemma and Figure 19.

Remark 3.5. The simple homological calculation in Remark 3.4 also implies the following observation. Let us assume that the $\mathrm{R2}_1$ move is realized. Then, the base diagram on the right hand side of Figure 20 must be homotopic to two parallel strands. Suppose that for this latter base diagram, the upper 1–handle slides over the lower one homologically r times. Then, by an argument similar to the above, we must have

$$\begin{aligned} \alpha + r\beta &= \varepsilon_1((\ell m + 1)\alpha + (k + m + k\ell m)\beta), \\ \beta &= \varepsilon_2(\ell\alpha + (k\ell + 1)\beta) \end{aligned}$$

for some $\varepsilon_1, \varepsilon_2 \in \{-1, +1\}$. By a straightforward calculation, we see that these equalities hold if and only if $\ell = 0$, $r = k + m$, $\varepsilon_1 = \varepsilon_2 = 1$. This means that the $\mathrm{R2}_1$ move is not always-realizable: for the realization, it is necessary that for $t \in [t_7, t_8]$, the upper 1–handle should not slide over the lower one at least homologically.

Remark 3.6. Let us assume that the base diagram on the left hand side of Figure 20 is transformed to a pair of vertical strands by homotopy. Then, we see easily that exactly the same argument as above leads to a contradiction.

4. Simplifying the topology of indefinite fibrations

In this section, we will give explicit algorithms for homotoping an indefinite fibration to a directed indefinite fibration, and in turn, to a directed indefinite fibration with embedded round image. Our algorithms will use base diagram moves which are always-realizable. These will consist of flip, unsink, push, Reidemeister type multi-germ moves gathered in Figure 21, and the additional *criss-cross braiding* move given in Proposition 3.3. We will also give similar algorithms for homotoping a directed indefinite fibration with embedded round image to one which is also fiber-connected and has connected round locus.

Note that for any one of the multi-germ moves in Figure 21, if the fibers over the given base diagram are all connected, then so are the fibers over the base diagram we get after applying the move. The only concern here can be for fibers over bounded regions formed after the move. However, in each case, one can reach to these regions from a region on the periphery by "going against the arrows", i.e. a fiber here is obtained by adding only 1–handles to a connected fiber on the peripheral region.

Lastly, recall that each time we get cusps during our homotopies, we apply the unsink move to turn them into Lefschetz singularities and then the push move to drag away the Lefschetz

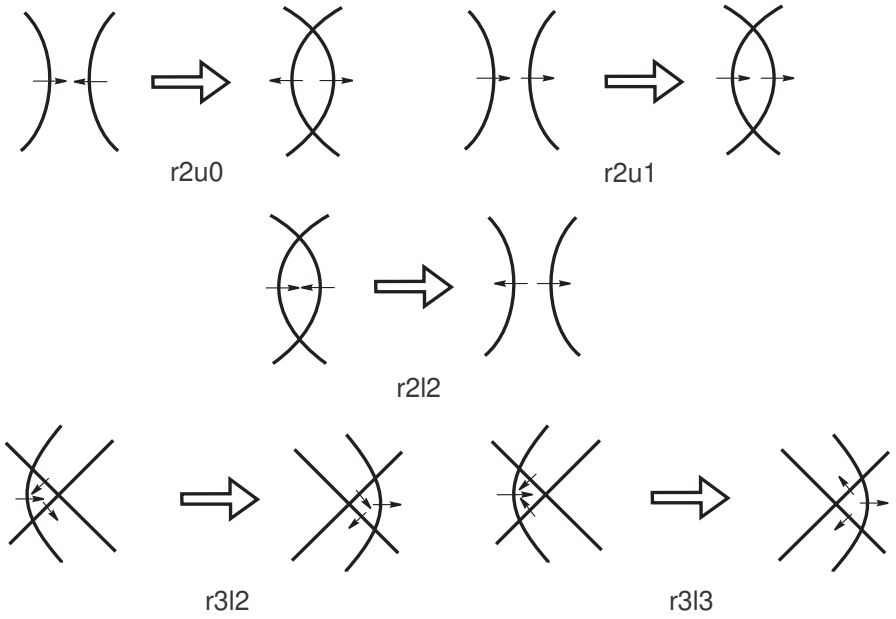

FIGURE 21. Several multi-germ moves that are always-realizable.

singularity to the higher genus side, away from where the rest of the action takes place. This is what we will be doing repeatedly throughout this section, without further mentioning it to save space.

4.1. **Immersed directed round image.**

We will now prove:

Theorem 4.1. *There exists a finite algorithm consisting of sequences of flip, unsink, push and Reidemeister type moves* $\mathrm{R2}^0$, $\mathrm{R2}^1$, $\mathrm{R2}_2$, $\mathrm{R3}_2$, $\mathrm{R3}_3$, *which homotopes any given indefinite fibration* $f\colon X \to D^2$ *to an outward-directed indefinite fibration* $g\colon X \to D^2$. *When* f *is fiber-connected, so is the resulting outward-directed indefinite fibration* g.

Note that all the moves mentioned in the above theorem are always-realizable. For an indefinite fibration over S^2, one can perform this algorithm over any fixed disk region on the base 2–sphere.

Proof of Theorem 4.1. Applying unsink moves, we may assume that f has no cusps. Take an embedded annulus $A = [0,1] \times S^1$ in D^2 which contains $f(Z_f)$ in its interior, and let $\pi\colon A \to S^1$ be the natural projection to the second factor. (Here $\{1\} \times S^1$ end of A is towards the interior of D^2). We may assume that $\pi \circ f|_{Z_f}$ is a Morse function and that the π–values of the crossings of $f(Z_f)$ are different than the critical values of $\pi \circ f|_{Z_f}$ in S^1. Let $t_1, t_2, \ldots, t_s \in S^1$ be the critical values of $\pi \circ f|_{Z_f}$, located in this order with respect to a fixed orientation of S^1, where a critical value may correspond to multiple critical points. Consider the "zones" $A_i = [0,1] \times [t_i, t_{i+1}] \subset A$, $i = 1, 2, \ldots, s$, where $[t_i, t_{i+1}] \subset S^1$ is the directed arc from t_i to t_{i+1}, and $t_{s+1} = t_1$. Then, $f(Z_f) \cap \operatorname{Int} A_i$ consists of a finite number of embedded and co-oriented vertical open arcs, where "vertical" means that π restricted to each open arc is a submersion. We say that such an arc is *positive* (resp. *negative*) if its co-orientation is consistent with the positive (resp. negative) direction of the $[0,1]$–factor of A_i. If necessary,

applying local isotopies as in Figure 22 in advance, we may assume that positive arcs do not intersect each other, in the expense of subdividing S^1 further.

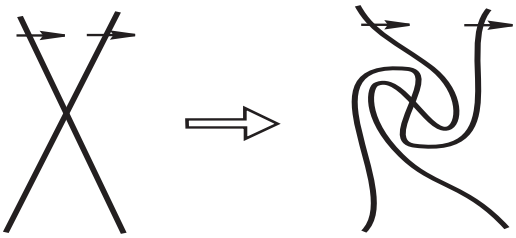

FIGURE 22. Turning an intersection of positive arcs into that of negative arcs.

Next, we will apply base diagram moves to f in such a way that, for the resulting indefinite fibration, all the arcs in each zone A_i are negative. We will continue to denote the resulting indefinite fibration by the same letter f, for simplicity. The following conditions will be preserved after each modification for each $i = 1, 2, \ldots, s$:

(1) Each arc in $f(Z_f) \cap A_i$ is vertical,
(2) Positive arcs in $f(Z_f) \cap A_i$ do not intersect each other.

Fix an index i. If A_i does not contain any crossing of $f(Z_f)$, then we can name the arcs of $f(Z_f) \cap \operatorname{Int} A_i$ as $\alpha_1, \alpha_2, \ldots, \alpha_r$ such that α_1 is situated in the rightmost position, and then α_2 is next to it on its left hand side, and so on. Suppose that $\alpha_1, \alpha_2, \ldots, \alpha_{\ell-1}$ are negative and α_ℓ is positive for some $1 \leq \ell \leq r$. When the end points of α_ℓ are not f–images of critical points of $\pi \circ f|_{Z_f}$, we apply the always-realizable multi-germ moves in Figure 21 together with pushes so that the move as depicted in Figure 23 is realized. As a result, the total number of positive arcs (in *any* A_i) decreases. During this procedure, the arc in question goes out of the annulus A temporarily, but in the end it is embedded in A *with negative co-orientation.* Note

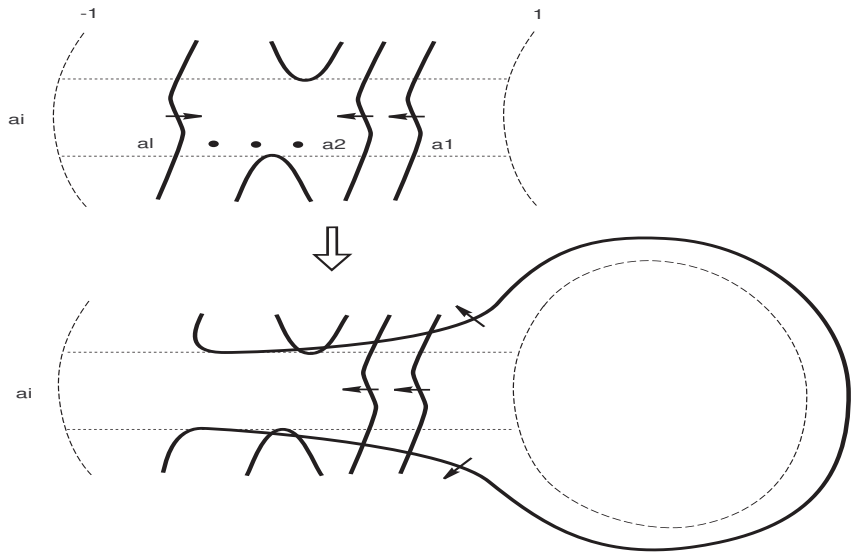

FIGURE 23. Moves that eliminate a positive arc: Part 1.

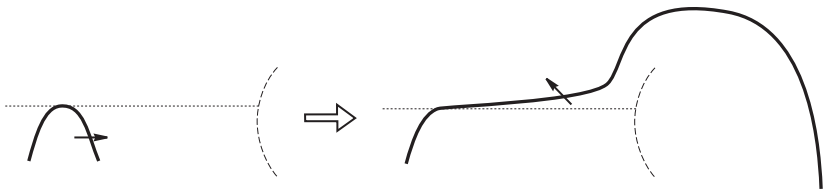

FIGURE 24. Moves that eliminate a positive arc: Part 2.

that the resulting base diagram still satisfies the above conditions (1) and (2); the number of arcs in A_j, $j \neq i$, increases, but they are all negative.

When an end point of α_ℓ is the f–image of a critical point of $\pi \circ f|_{Z_f}$, we apply the sequences of moves as depicted in Figure 24 or in Figure 25, which consist of the always-realizable multi-germ moves in Figure 21 and pushes, as well as a flip and a pair of unsinks in the latter case. Note that in Figures 24 and 25, only the moves performed around the upper part of the zone A_i are depicted, and the moves in the hidden lower part are performed as in Figure 23.

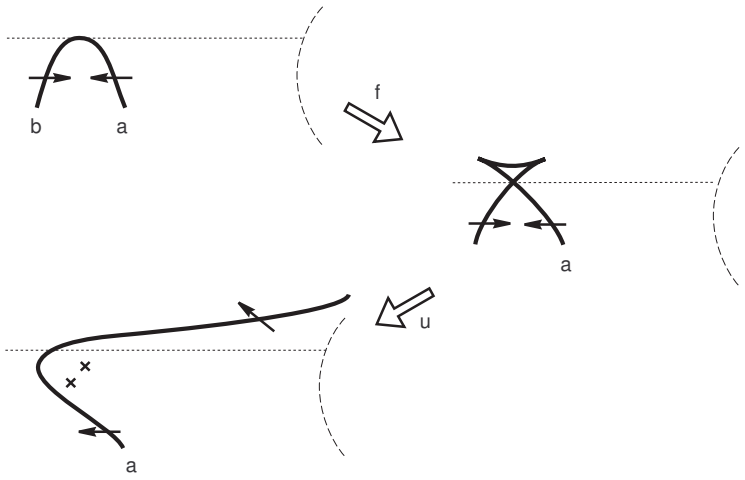

FIGURE 25. Moves that eliminate a positive arc: Part 3.

Now consider the case when A_i contains crossings of $f(Z_f)$. Let $\alpha_1, \alpha_2, \ldots, \alpha_r$ be the (open) vertical arcs of $f(Z_f) \cap \operatorname{Int} A_i$. If they are all negative, then we have nothing to do. Suppose some are positive. Say α_ℓ is the rightmost positive vertical arc; i.e. there are no positive vertical arc components in the right hand side region of $\operatorname{Int} A_i \setminus \alpha_\ell$. (Note that if there are positive vertical arcs, then such α_ℓ exists, since we made sure that positive arcs do not intersect.) On α_ℓ, there may be intersections with negative arcs. If there is no crossing in the right hand side region, then we can apply moves similar to those used above to decrease the number of positive arcs. Otherwise, all the crossings in the right hand side region of $\operatorname{Int} A_i \setminus \alpha_\ell$ involve only negative arcs. When we move α_ℓ to the right using moves as described above, it may encounter such a crossing of negative arcs. In that case, we get a triangular region such that one edge is on α_ℓ and the other two are on negative arcs. We may assume that the edges are line segments, which are never horizontal. If the "height" of the vertex of this triangle that is not on α_ℓ is between the heights of the other two vertices, then we have a situation

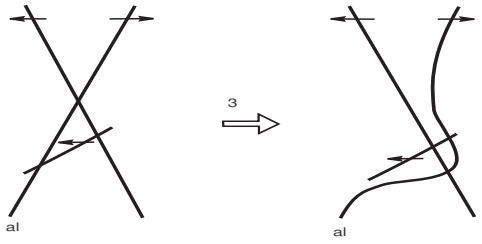

FIGURE 26. Moves that eliminate a positive arc in A_i: Part 4.

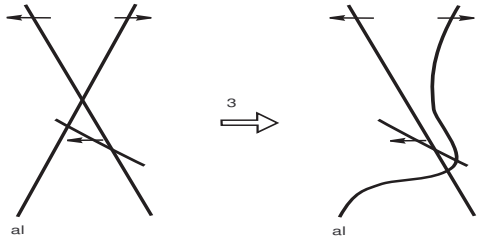

FIGURE 27. Moves that eliminate a positive arc in A_i: Part 5.

as described in the left hand side picture of Figure 26. In this case, we can apply the move $\mathrm{R3}_3$ to decrease the number of crossings in the right hand side region. If that vertex is lower (or higher) than the other two vertices, then we get the left hand side picture of Figure 27, and we can apply the move $\mathrm{R3}_2$.

Then, by the same argument as above, we can finally eliminate the positive arc α_ℓ. Note that after the moves, both conditions (1) and (2) are maintained.

Applying these procedures to the positive arcs of $f(Z_f) \cap \operatorname{Int} A_i$ from right to left, we can eliminate all the positive arcs in $\operatorname{Int} A_i$, for each $i = 1, 2, \dots, s$. Finally, we get an indefinite fibration g where all arcs in $g(Z_g) \cap \operatorname{Int} A_i$ are negative for all $i = 1, 2, \dots, s$, which means that the resulting indefinite fibration g is outward-directed.

Note that our whole algorithm was performed away from the boundary of the base disk D^2, where the resulting round image is directed outwards. So if a regular fiber F of f over ∂D^2 was connected, then *all* fibers of g are connected: they are derived by fiberwise 1–handle attachments from F. In particular, g is fiber-connected if f is. □

4.2. **Embedded directed round image.**

In this subsection, we assume that the closed orientable 4–manifold X is connected, and we prove:

Theorem 4.2. *There exists a finite algorithm consisting of sequences of flip, unsink, push, criss-cross braiding and Reidemeister type moves* $\mathrm{R2}^0$, $\mathrm{R2}^1$, $\mathrm{R2}_2$, $\mathrm{R3}_2$, $\mathrm{R3}_3$, *which homotopes any given directed indefinite fibration* $f\colon X \to S^2$ *to a fiber-connected and directed indefinite fibration* $g\colon X \to S^2$ *with embedded round image.*

Proof. Below, as we modify the map f through homotopies, we will keep denoting the resulting map with the same letter.

Since f has immersed directed image, we can view the round image $f(Z_f)$ to be braided around, say the north pole, directed towards it. That is, we regard $f(Z_f)$ as the closure of

a virtual braid on m strands. We will call it the *base braid* for f. For convenience, we will think of $f(Z_f)$ as the union of a base braid, given by a virtual braid diagram as in Figure 28, and a trivial braid, where the latter is end summed to the former to recapture the round image $f(Z_f)$ as the braid closure.

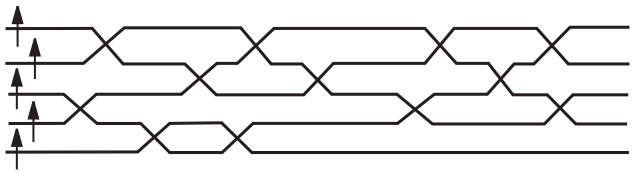

FIGURE 28. An example of a base braid diagram on 5 strands. The round image is its closure, which is obtained by end summing the base braid with a trivial braid on 5 strands.

First, we will show that the fibers over the southernmost region of $S^2 \setminus f(Z_f)$ are connected. Let $A \cong S^1 \times [-1,1]$ be an annular neighborhood of $f(Z_f)$, where the interval $[-1,1]$ points north. So $S^2 \setminus A = N_{\mathrm{NP}} \sqcup N_{\mathrm{SP}}$, where N_{NP} and N_{SP} denote open 2–disk neighborhoods of the north and south poles, respectively. The images of all the Lefschetz critical points are contained in N_{SP}. We can assume that the map $\pi_{S^1} \circ f|_{Z_f} \colon Z_f \to S^1$ is a submersion, where, under the identification $A \cong S^1 \times [-1,1]$, $\pi_{S^1} \colon S^1 \times [-1,1] \to S^1$ is the projection to the first factor. Then, X is decomposed into three compact 4–manifolds $f^{-1}(\overline{N}_{\mathrm{NP}})$, $f^{-1}(\overline{N}_{\mathrm{SP}})$ and $f^{-1}(A)$. Note that $f^{-1}(\overline{N}_{\mathrm{NP}})$ is a trivial surface bundle over $\overline{N}_{\mathrm{NP}}$, while $f^{-1}(A)$ is a fiber bundle over S^1 with fiber $Y = f^{-1}(\mathrm{pt}) \times [-1,1])$, where Y is a 3–manifold obtained from $f^{-1}(\mathrm{pt} \times [1-\varepsilon, 1])$, $0 < \varepsilon << 1$, by attaching m 1–handles. Suppose the fibers are disconnected over N_{SP}. The 3–manifold $f^{-1}(\partial \overline{N}_{\mathrm{SP}})$ is a fiber bundle over S^1 with fiber surface, say S, with monodromy generated by Dehn twists. Therefore, the monodromy diffeomorphism preserves each connected component of S. Then, for the Y–bundle over S^1, $f^{-1}(A)$, the monodromy also preserves each connected component of Y. Therefore, by attaching $f^{-1}(\overline{N}_{\mathrm{NP}})$ and $f^{-1}(\overline{N}_{\mathrm{SP}})$ to $f^{-1}(A)$, we get a disconnected 4–manifold, which is a contradiction. Thus, the fibers over N_{SP} are necessarily connected.

We can now give our algorithm to prove the theorem. If $m = 0$ or 1, then there is nothing to do, so we assume there are $m \geq 2$ strands.

Step 1: As we have shown above, the fibers over the points in the southernmost region of $S^2 \setminus f(Z_f)$ are connected. Using the R2[1] moves, we can locally pull down a pair of parallel strands towards the south pole, so that we get a pair of parallel strands such that the lower one is adjacent to the southernmost region (see the middle diagram of Figure 29). Then, by a criss-cross braiding move of Proposition 3.3, we can locally replace the pair of parallel strands with a pair of strands that have three mutual crossings (see the rightmost diagram of Figure 29), while modifying the round locus above it. This modification acts as a transposition on the m points the virtual braid is moving around. Since the symmetric group of m points is generated by transpositions, by adding enough crossings, the base braid for the new round image $f(Z_f)$ becomes a *pure* virtual braid. The new round locus Z_f has exactly m connected components.

Using always-realizable base diagram moves, we will turn this pure virtual base braid on m strands into a trivial braid on m strands. As we will keep the normal directions on all strands, the result will also be a directed indefinite fibration, but with embedded round image.

Step 2: Recall that all the Lefschetz singularities are away from the base diagram, contained in a small open disk neighborhood N_{SP} of the south pole, which we will regard as the point

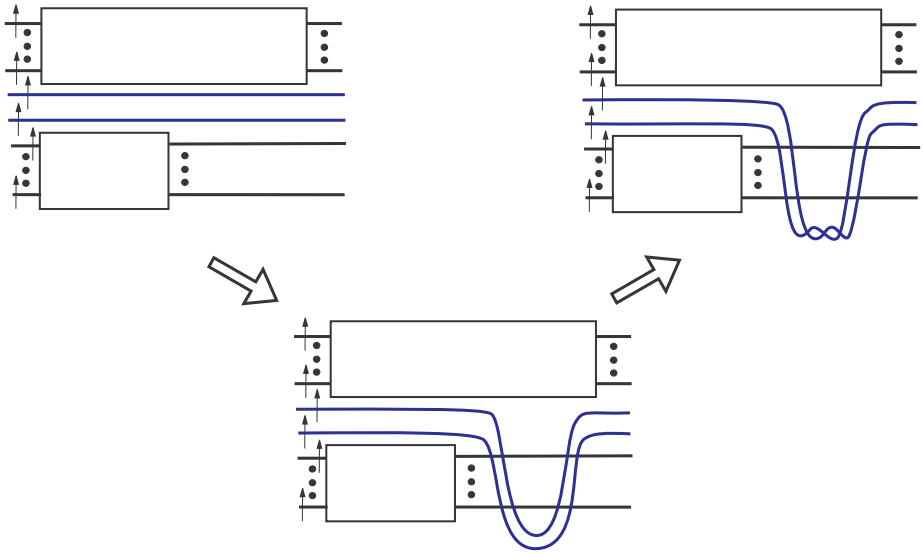

FIGURE 29. $R2^1$ moves followed by criss-cross braiding. In the small boxes, we may have any braid (on the corresponding number of strands).

at infinity. The only time our modifications will involve this neighborhood is when we will swing a subarc of a round image component over the south pole. In this case we will always have the normal arrow on the arc pointing towards the south pole when we begin sliding it. So we can push all the Lefschetz singularities against it to continue the slide. For these reasons, we will not discuss Lefschetz singularities any further.

Regard the base braid diagram of our pure virtual braid as a simultaneous graph of m continuous functions $[0,1] \to (0,1)$. Take the strand b whose end points are in the top most position; we will refer to it as the *top strand*. Each time it has a local minimum (resp. a local maximum) in the interior, by using $R2^1$ move repeatedly, pull it down (resp. raise it up) — while avoiding braid crossing— until it becomes a global minimum (resp. global maximum); see Figure 30. Repeat this for every local minimum and maximum of the same strand, until any local minimum/maximum b has is a global minimum/maximum. The number of crossings may increase drastically during this procedure!

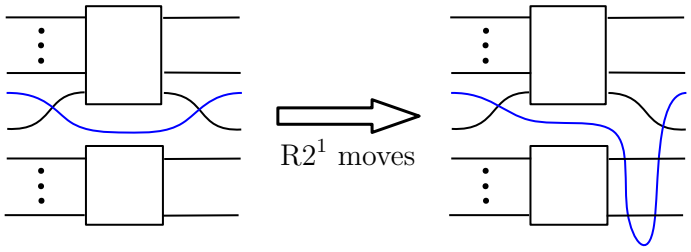

FIGURE 30. Lowering a local minimum of a strand (shown in blue) to a global minimum position. Normals to all strands are directed towards the top. In the two small boxes, we may have any braids (on the corresponding numbers of strands).

While the new crossing pattern between the strand b we pulled around and the rest of the braid is clear, in between every consecutive global maxima (or minima) of b, lies some possibly highly non-trivial —and not necessarily pure— virtual braid on $m-1$ strands, which is split from our strand. We keep each one of these subbraids on $m-1$ strands in a box; see Figure 31. Moreover, we can use the braid closure to bring the boxes on the far left and far right together, and regard it as a single box. The closure of the resulting braid is shown in Figure 31, with normals to all strands still directed towards the north pole.

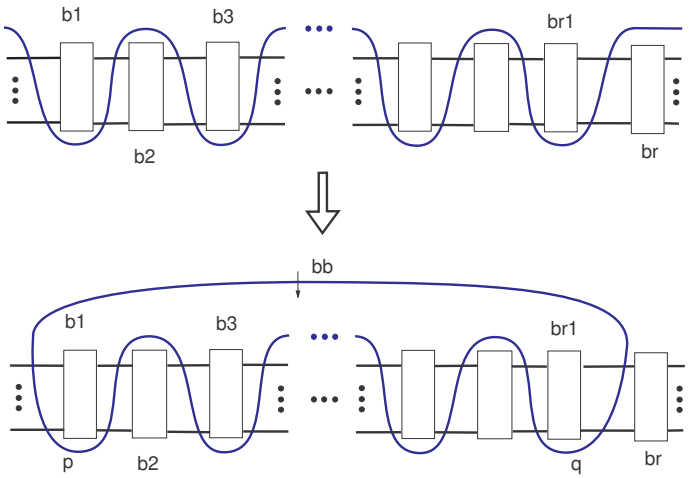

FIGURE 31. Strand b, depicted by blue, and the other strands made up with braid boxes $B_1, B_2, \ldots, B_{2r}$ (Top). Then, we slide the sub-strand b' of b over the north pole (Bottom).

Observe that the number of boxes we have at the end is even; say $2r$. Here $r = 0$ means the top strand b, and thus its closure $\hat{b}$, the innermost component of Z_f (with respect to the north pole), do not intersect the others. In this case, we can isotope it into a small open disk neighborhood N_{NP} of the north pole. Any arc we swing over the north pole with its normal arrow directed towards the north pole can go past this component by an $\mathrm{R2}^1$ move followed by an $\mathrm{R2}_2$ move (see Figure 32).

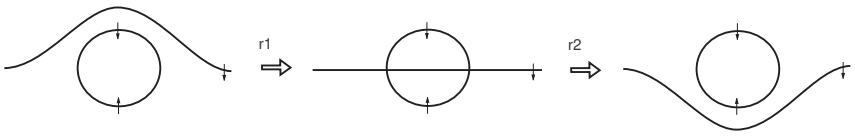

FIGURE 32. Round image can go through an inward directed embedded circle by an $\mathrm{R2}^1$ move followed by an $\mathrm{R2}_2$ move.

Now, our strategy is the following. If the top strand is embedded (i.e., when $r = 0$), it will be pushed into N_{NP}. Otherwise (i.e., when $r > 0$), we do a bunch of moves to make it embedded and push it into N_{SP} instead. We then start over with the new top strand and repeat until all strands are embedded and non-nested.

Let us proceed to the case $r > 0$. Let p and q be the two global minimum points on b closest to the ends of the strand b in the diagram. (If there is only one global minimum, flatten the strand around it, so p and q are distinct points.) During the next modifications,

we will temporarily ruin the braid picture, and will only consider the base braid as a *portion* of the round image $f(Z_f)$. Take the complement b' of b in its closure $\hat{b}$. Slide b' over the neighborhood N_{NP} of the north pole so it approaches the non-trivial braid from the top; see Figure 31. The crucial point here is that b' is directed *against* all the braid components, so after several $\mathrm{R2}^0$, $\mathrm{R2}_2$, and $\mathrm{R3}_3$ moves (many of them involving b as well), we can pull b' all the way down, below any of the other braid strands (including minima of b), except for two kinks we unavoidably get around p and q on b. See the top diagram of Figure 33. During these Reidemeister moves, we fix the base braid, except for the far left and far right $m-1$ crossings of b with other strands we eliminated when lowering b (as we pulled b' down) at the ends.

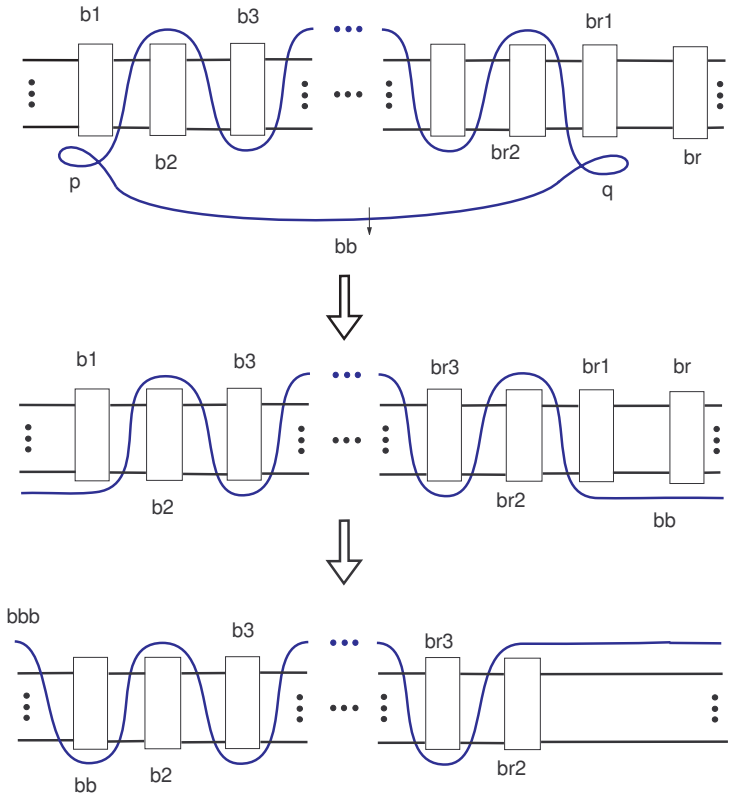

FIGURE 33. We lower b', swing it over the south pole (while pushing the Lefschetz critical points across it), and rearrange the braid boxes B_{2r-1}, B_{2r} and B_1 into one.

After introducing a flip, and then applying $\mathrm{R2}_2$ and unsink moves, we can get rid of each kink as shown in Figure 34. So we can continue pulling b' and swing it over the south pole in order to bring it again to the other side of the base diagram. It now completes the missing strand of the trivial braid portion.

So we have a new base braid on m strands, which represents the new round image $f(Z_f)$. The bottom strand came from sliding b', whereas the rest of the braid diagram is the same as before (see the middle diagram of Figure 33). As we get ready to repeat the whole procedure, we first observe that the bottom strand already has only global extrema. More importantly, we now have 2 boxes on one side and 1 box on the other side which do not have the bottom

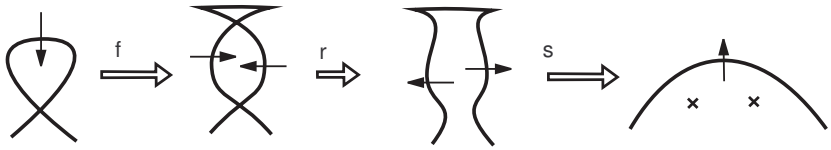

FIGURE 34. Getting rid of the kinks.

strand going in between. Using the braid closure as before, we can slide them into one box. We now have $2(r-1)$ boxes in total (see the bottom diagram of Figure 33, where $B_{2r-1}B_{2r}B_1$ should mean B_1B_2 when $r=1$).

If the new number of boxes is not zero, then it means we still have some global maximum. Then, isotoping the round image, we can place the same component of $f(Z_f)$ in the braid diagram so that it is in the top position again. Hence, repeating the procedure $r-1$ more times, we arrive at a base braid with a bottom strand split from the others.

For one last time, we slide the complement b' of the new top strand b over the north pole and across the braid diagram. Though this time we bring it below the rest of the braid diagram but keep it above b (creating no kinks), so the round image component $b \cup b'$ is embedded and encloses a disk region without any singularities (see Figure 35). Its normal arrow is directed towards the interior of the disk. We can isotope this component of the new round image $f(Z_f)$ into the small neighborhood N_{SP} of the south pole, next to the Lefschetz singularities. As it was the case for a component we isotoped into N_{NP}, any arc we swing over N_{SP} with its normal arrow directed towards the south pole can go past this component by an $\mathrm{R2}^1$ move followed by an $\mathrm{R2}_2$ move (see Figure 32).

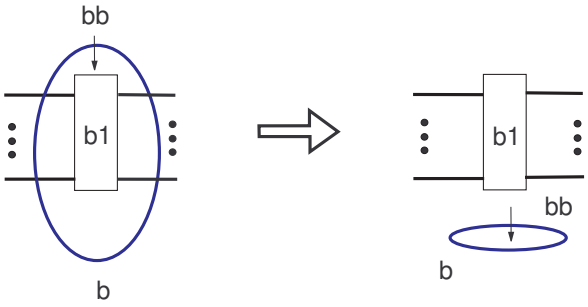

FIGURE 35. Last time we lower the strand b'.

Step 3: With our remarks on the singular image isotoped into $N_{\mathrm{NP}} \cup N_{\mathrm{SP}}$ in mind, we can run *Step 2* for the remaining virtual braid on $m-1$ strands. Repeating it $m-2$ times, we obtain a new indefinite fibration f with embedded singular image. The singular image of f is now contained in the two open disks N_{NP} and N_{SP}, with $f(Z_f)$ consisting of m split components (i.e. no two are nested). We view all in a large disk D as shown on the left hand side of Figure 36 below. Recall that the fiber over the south pole was connected. So the fiber over the south pole after Steps 1–2 is still connected: as we swung several indefinite fold arcs over this point, we only added 1–handles to it. It follows that the regular fibers over the boundary of the disk D are connected.

Step 4: Here we apply the *flip and slip move* of [5, Fig. 5], to turn an inward-directed circle in D inside out, so it becomes outward-directed (see Figure 9 in Subsection 3.3).

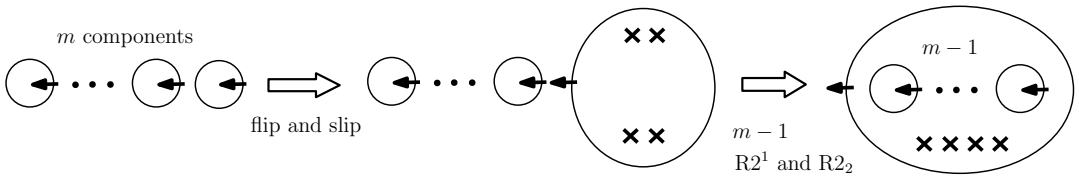

FIGURE 36. From split round image back to directed.

Apply flip and slip to the far right circle so it is now outward-directed. By exactly $m-1$ $\mathrm{R2}^1$ and $m-1$ $\mathrm{R2}_2$ moves again, we can pull the left half of the circle all the way to the left, so it now encloses all the other circles; see Figure 36. Repeating this procedure $m-2$ times for the split collection of circles contained inside, we arrive at a nested collection of outward-directed, embedded round image circles. All the Lefschetz singularities we had and produced during this process can be pushed into the innermost round image circle.

This is the base diagram for the resulting directed indefinite fibration $g\colon X \to S^2$ with embedded round image. Because the regular fibers over ∂D are connected, and because all the others are obtained from them by fiberwise 1–handle attachments and Lefschetz handle attachments, the indefinite fibration g is fiber-connected. □

It can be seen from the proof that the cost of passing from immersed to embedded round image is the increase in the number of Lefschetz critical points, as well as the fiber genera.

Remark 4.3. Theorems 4.1 and 4.2 together show that given any map from a closed orientable 4–manifold to S^2, we can homotope it to a generic map with embedded singular image. The corresponding statement is not true for an arbitrary map from a 3–manifold to S^2 (or to other surfaces); there are obstructions to getting a generic map with embedded singular image within the same homotopy class [19, 30, 69]. Similarly, there are obstructions for maps from 4–manifolds to 3–manifolds [72]. In this regard, maps from $n \geq 4$ dimensional manifolds to S^2 seem rather special.

4.3. **Connected fibers and connected round locus.**

Here we will prove the following proposition, which, together with Theorems 4.1 and 4.2, provides a sequence of base diagram moves to homotope any given indefinite fibration over S^2 to one that is fiber-connected and has connected round locus –in short, *simplified*.

Proposition 4.4. *Let X be a connected 4–manifold. There exists a finite algorithm consisting of sequences of flip, unsink, push, cusp merge, and Reidemeister type moves* $\mathrm{R2}^1$ *and* $\mathrm{R2}_2$*, which homotopes any given inward-directed indefinite fibration $f\colon X \to D^2$ with embedded round image to a fiber-connected outward-directed indefinite fibration $g\colon X \to D^2$ with embedded round image and connected round locus.*

Proof. Observe that since X is connected, even if there are disconnected fibers, the regular fibers over ∂D^2 should be connected.

The first part of the algorithm is the same as in Steps 2–3 of our proof of Theorem 4.2, carried out in much simpler case of a pure virtual braid. (Note that these homotopies in these steps can all be performed over D^2.) We first push out all the Lefschetz singularities so they are near the boundary of the disk, and do not interfere with all the other moves we will perform. Assume that there are $m > 1$ components. By exactly $m-1$ $\mathrm{R2}^1$ and $m-1$ $\mathrm{R2}_2$ moves, we can pull out the right half of the outermost circle all the way left, so it is now

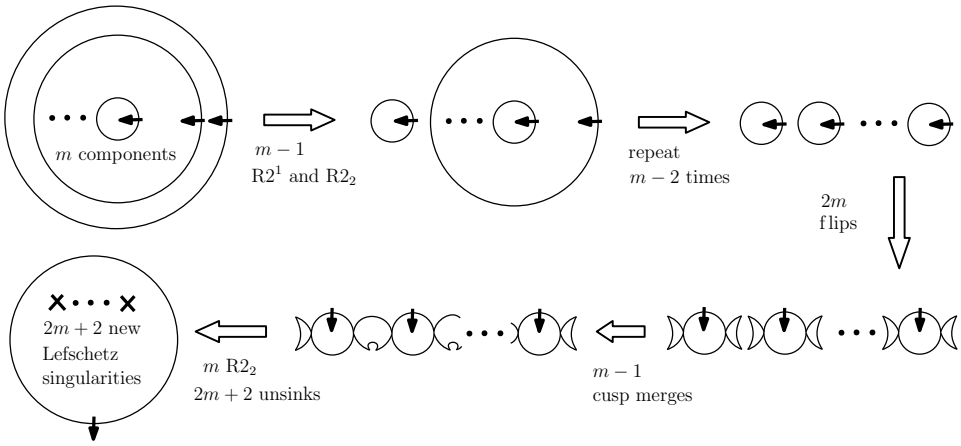

FIGURE 37. Making fibers and the round locus connected.

disjoint from the rest. Repeating this $m-2$ times for the next outermost circle of the nested circles each time, we arrive at a split collection of m inward-directed embedded circles as in the top row of Figure 37.

Now flip each circle twice, and then merge all into one immersed circle by $m-1$ cusp merges as shown in Figure 37. (Note that these cusp merges are realizable, since the fibers over points near the boundary are all connected.) This is followed by m $R2_2$ and $2m+2$ unsink moves to arrive at an outward-directed embedded round image, where the resulting indefinite fibration $g\colon X \to D^2$ has connected round locus. Once again, it is fiber-connected, since all the fibers are obtained by fiberwise 1–handle attachments and Lefschetz handle attachments. □

Remark 4.5. The procedures we have given in Theorem 4.1, in Step 1 of Theorem 4.2 and in Proposition 4.4 can all be applied in a more general setting. Let X be a compact oriented 4–manifold with corners, Σ be a compact oriented surface with boundary, and $f\colon X \to \Sigma$ be an indefinite fibration such that

- $\partial X = P \cup Q$, where P and Q are compact codimension zero submanifolds of ∂X and are glued along $\partial P = \partial Q = P \cap Q$,
- X has corners exactly along $\partial P = \partial Q$,
- $f^{-1}(\partial\Sigma) = Q$,
- $f|_Q\colon Q \to \partial\Sigma$ and $f|_P\colon P \to \Sigma$ are submersions.

In particular, when $\Sigma = D^2$, we have a naturally induced open book structure on ∂X. The moves we have described can be seen to work for such an indefinite fibration as well. For birth/death, flip/unflip, fold merge, criss-cross braiding, and Reidemeister type moves, the handlebody arguments we used are implicitly based on ascending and descending manifolds for gradient-like vector fields (for example, see [27]). Let us take an embedded arc α in Σ which is transverse to f. Then, $f|_{f^{-1}(\alpha)}\colon f^{-1}(\alpha) \to \alpha$ is a Morse function. As f is a submersion on P, the fibers of f are compact surfaces with boundary and this Morse function is a submersion on the closure of the boundary of $f^{-1}(\operatorname{Int}\alpha)$. So we can choose a gradient-like vector field that is tangent to the boundary. This means that an integral curve never hits the boundary (except along $f^{-1}(\partial\alpha)$) as long as we start from an interior point. Therefore, the above mentioned moves can be realized by exactly the same method as before. Unsink, push, cusp merge, wrinkle, and C-moves are easily seen to be realizable as well.

5. Realizing a prescribed 1–manifold as the round locus

The purpose of this section is to show that any null-homologous 1–dimensional embedded closed oriented submanifold Z of X, with any prescribed twisting data satisfying a certain necessary condition (for the local models around components) can be realized as the round locus Z_f of a fiber-connected, directed broken Lefschetz fibration $f\colon X \to S^2$ with embedded round image.

First, we note a couple observations on the round locus of a broken Lefschetz fibration/pencil, which will naturally appear as necessary conditions for our arguments to follow. Analogous statements for the zero loci of near-symplectic structures are well-known [66], so one can also appeal to [4] to build a near-symplectic form whose zero locus is the same as the round locus, and translate these results. We will instead sketch parallel arguments in the realm of indefinite fibrations.

Proposition 5.1. *Let $f : X \to \Sigma$ be an indefinite fibration, where X and Σ are closed. Then, Z_f is a closed 1–dimensional submanifold of X which is canonically oriented. Furthermore, Z_f is null-homologous, i.e., $[Z_f] = 0$ in $H_1(X;\mathbb{Z})$.*

Proof. If there are Lefschetz singular points, then use a wrinkling move to perturb each Lefschetz singular point into an indefinite singular circle with 3 indefinite cusps. Born in a 4–ball, each one of these circles is null-homologous. Thus we may as well assume that f is an indefinite generic map. Then by [3, §4], the singular point set Z_f of f is orientable. Furthermore, the cohomology class dual to $[Z_f] \in H_1(X;\mathbb{Z})$ is calculated in [3, §5]. Although it is not explicitly written there, we can show that the Poincaré dual of $[Z_f] \in H_1(X;\mathbb{Z})$ coincides with the integral Stiefel–Whitney class $W_3(X) \in H^3(X;\mathbb{Z})$ as follows. First, note that the relevant cohomology class corresponds to one in $H^3(BSO;\mathbb{Z})$, a characteristic class. As is remarked in [3, Remark 5.5], the $\mathbb{Z}_2$–reduction of the dual cohomology class coincides with the Stiefel–Whitney class w_3 in $\mathbb{Z}_2$–coefficients. On the other hand, an element of $H^3(BSO;\mathbb{Z})$ is mapped to w_3 by the modulo 2 reduction if and only if it is of the form $W_3 + 2P$, where P is a certain polynomial in Pontrjagin classes (see [15], for example). As we are in degree 3, P must vanish, and therefore the relevant class must be equal to W_3.

Now W_3 is the obstruction to admitting a spin^c structure, and it vanishes on a closed oriented 4–manifold X; see [39, §4], [77]. □

Proposition 5.2. *Let $f\colon X \to \Sigma$ be a broken Lefschetz fibration, where X and Σ are closed and connected. Then, the number of untwisted (even) components of Z_f has the same parity as $1 + b_1(X) + b_2^+(X)$.*

Proof. Here is a proof similar to the one given in [66] for near-symplectic forms. Given a Riemannian metric on X, we can naturally construct an almost complex structure on $X \setminus Z_f$. Off the Lefschetz critical points, we define the almost complex structure as the rotation of $\pi/2$ on the tangent planes to the regular part of fibers and also on the normal planes. Around Lefschetz critical points, this is modified to match the complex structures coming from the local models. Then, the obstruction to extending the above almost complex structure to whole of X coincides with both the number of untwisted circles in Z_f and $1 + b_1(X) + b_2^+(X)$ modulo 2 [66]. □

We can now prove the main result of this section:

Theorem 5.3. *Let X be a closed connected oriented 4–manifold and Z be a (non-empty) null-homologous closed oriented 1–dimensional submanifold of X. There exists a finite algorithm consisting of sequences of always-realizable moves flip, cusp merge, unsink, push,*

criss-cross braiding, C-move, $\mathrm{R2}^0$, $\mathrm{R2}^1$, $\mathrm{R2}_2$, $\mathrm{R3}_2$ *and* $\mathrm{R3}_3$*, which homotopes any given indefinite fibration* $f\colon X \to S^2$ *with non-empty round locus to a fiber-connected, directed broken Lefschetz fibration* $g\colon X \to S^2$ *with embedded round image, whose round locus* Z_g *coincides with* Z *as oriented* 1*–manifolds. Moreover, for any prescribed twisting data for* Z*, with number of untwisted components congruent modulo* 2 *to* $1 + b_1(X) + b_2^+(X)$*,* g *can be chosen so that* Z_g *and* Z *have matching twisting data.*

Proof. Take the indefinite fibration f on X, and apply the procedures we presented in the proofs of Theorems 4.1 and 4.2 to get a *directed* indefinite fibration with *embedded* round image. We can also make it fiber-connected and with connected round locus by applying the procedure given for Proposition 4.4. Note that since the base is S^2, each time we have an inward-directed or an outward-directed image, we also have the other. At the end, we have a fiber-connected indefinite fibration with embedded and connected round image, which we will continue to denote by f. We can also assume that f has no cusps by applying unsink moves. In the following, we will modify f step by step. For simplicity, after each step, we continue to denote the resulting map by the same symbol f.

Let F denote the highest genus regular fiber. Then, the inclusion $i\colon F \to X$ induces an epimorphism $i_*\colon \pi_1(F) \to \pi_1(X)$, as seen from the handlebody decomposition of X induced by the broken Lefschetz fibration f [6]. (The kernel is normally generated by the vanishing cycles of the round 2–handle and Lefschetz 2–handles, together with the attaching circle of one more 2–handle pulled from the lower side.)

Now, by applying the moves as in Figure 38, we can make prescribed components in Z_f in such a way that all but one component of Z_f are isotopic to the corresponding components of Z. These are mainly base diagram moves, except we pay additional attention to how we perform cusp merges: we merge them along paths which approximate the components of Z we would like to realize. Also, we first assume that the component of Z in question is isotoped so that the restriction of f to it is already an embedding, the image of which is given by a blue circle in the figure. (This is achieved by representing the homotopy class of the component by a loop γ in a highest genus fiber F and then by perturbing it to the loop defined by $S^1 \ni t \mapsto (\gamma(t), t) \in F \times S^1$, where S^1 is a small embedded circle in the base surface and $F \times S^1 = f^{-1}(S^1)$.) Note that the path for each cusp merge move, the projection of which is depicted by a dotted line, lies in a region corresponding to the highest genus region before the preceding flip. Therefore, we can adjust the homotopy classes (and hence the isotopy classes) of the components of Z_f corresponding to the blue circles, by the surjectivity of i_* mentioned above. The process indicated by the letter "P" in Figure 38 consists of a repetition of the preceding operations.

By assumption, Z is null-homologous, and so is Z_f by Proposition 5.1. Since we already matched all but one components, the remaining component of Z_f is $\mathbb{Z}$–homologous to the remaining component of Z. Then, the difference of these remaining components, as an element of the fundamental group $\pi_1(X)$ is a product of finitely many commutators, again surjected from $\pi_1(F)$. By applying the base diagram moves as in Figure 39, we can adjust the last component of Z_f by one commutator at a time, say $[\alpha, \beta] = \alpha\beta\alpha^{-1}\beta^{-1}$. Note that in the blue box in Figure 39, we have concentric inward-directed circles together with Lefschetz critical values. Here $\tilde{R}$ in Figure 39 consists of an iteration of pushes, moves $\mathrm{R2}^1$ and moves $\mathrm{R2}_2$, which are always-realizable. At the final stage, we apply the unsinks eight times to get the image $f(Z_f) \cup f(C_f)$ exactly the same as the original one except for the Lefschetz critical values. However, the position of Z_f in X has been changed in such a way that the homotopy class of the final component has been changed by a commutator.

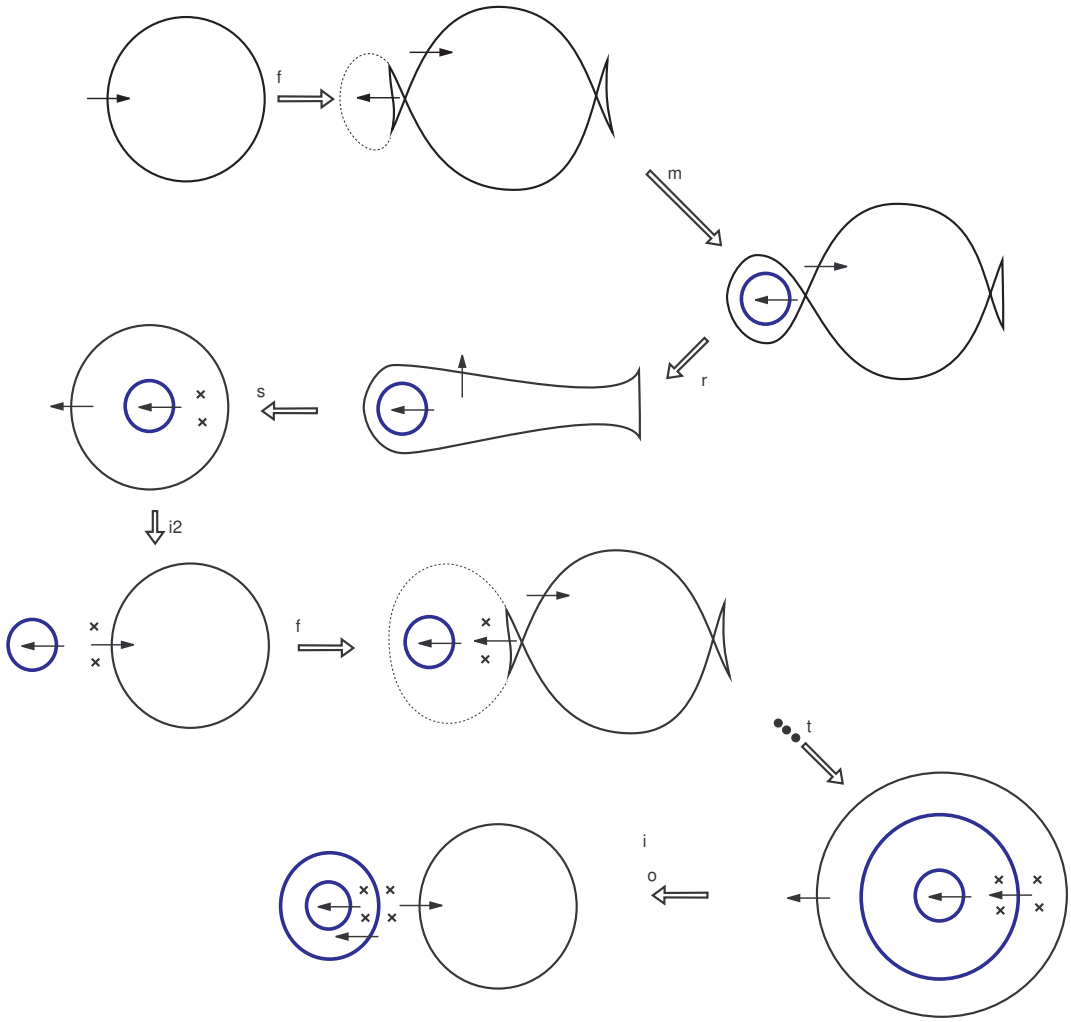

FIGURE 38. Realizing prescribed components, whose images are depicted by blue circles.

By repeating this procedure, we arrive at a broken Lefschetz fibration $g\colon X \to S^2$ with directed embedded image and with $Z_g = Z$, which is homotopic to the original f through always-realizable moves listed in the statement of the theorem. This proves the first part of our claim.

As for matching the twisting data, we need to slightly modify the above proof. Note that the condition on the number of untwisted components is necessary by Proposition 5.2.

In order to adjust the homotopy class of a new born component, we used a cusp merge along a joining curve in the highest genus region. Given such a curve, we have some freedom for performing the cusp merge [55, 14]. As seen in the proof of (4.8) Lemma (1) or (4.6) Lemma (2) in [56], an appropriate set of coordinates is chosen in a neighborhood of the joining curve. The choice is, in a sense, canonical, except that we have some freedom to choose coordinates along fibers. More precisely, we can change the coordinates z according to the parameter u, borrowing the notation from [56]. If we choose the coordinates z in such a way that it is "rotated by π" along the parameter u, then the result of the cusp merge looks

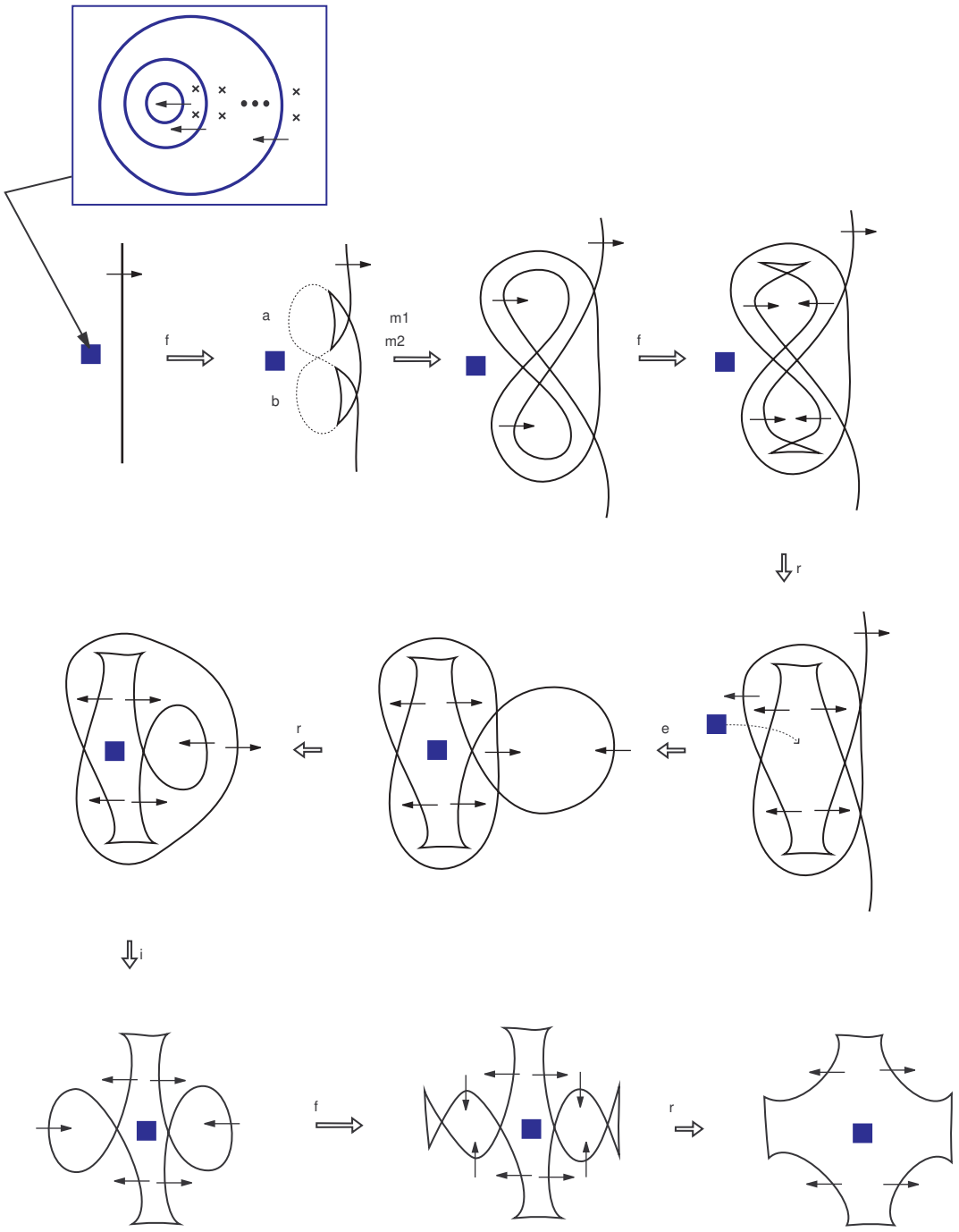

FIGURE 39. Adjusting the last prescribed component.

the same; however, the local data changes along the two new born arcs. (In the terminology of proof of [55, Theorem 6.1] or in the argument in the last part of merging move in Section 3 of [55], we can rotate the 2–disks embedded in the fibers along the horizontal curve connecting the two Lefschetz critical points.) Using this technique, we can adjust the twisting data of the

new born component. We continue the same process until we get the final component. The twisting data of this last component *will be* the same as the twisting data of the corresponding component of Z, since the number of untwisted components of both have the same parity, namely, $1 + b_1(X) + b_2^+(X)$ modulo 2. □

Remark 5.4. We can remove the condition $Z_f \neq \emptyset$ from Theorem 5.3 by allowing an initial birth move; otherwise, our procedure features no births or death moves. A similar realization is also possible for generic maps into surfaces; see [68].

6. Constructions of broken Lefschetz fibrations and pencils

We now present purely topological constructions of broken Lefschetz fibrations and pencils with simplified topologies. These algorithmic constructions improve on the procedures given by the authors in [70, 5], by incorporating the new procedures we have obtained in the previous sections.

First is the construction of broken Lefschetz fibrations on arbitrary 4–manifolds:

Theorem 6.1. *Let X be a closed connected oriented 4–manifold and Z be a (non-empty) null-homologous closed oriented 1–dimensional submanifold of X, given with a prescribed twisting data, in which the number of untwisted (even) components has the same parity as $1 + b_1(X) + b_2^+(X)$. Then, there exists a fiber-connected, directed broken Lefschetz fibration $f\colon X \to S^2$ with embedded round image, whose round locus Z_f matches Z with the same local models. Given any generic map from X to S^2, such f can be derived from it by an explicit algorithm.*

Proof. Let $h\colon X \to S^2$ be a generic map, which always exists [57, 73, 77]. It has only fold and cusp singularities, but the 1–dimensional singular locus might include definite folds. If that is the case, then we homotope h to an indefinite generic map $f\colon X \to S^2$ using an algorithm given by the second author in [70] (also see [71]). This procedure is given by moves similar to the ones we have discussed here, but now they involve *definite* folds as well: always-realizable flip, cusp–fold crossing, birth–death, and Reidemeister type moves, together with cusp merge and fold merge moves that can be realized algorithmically.[2] An alternate proof for eliminating the definite fold, which also goes through a sequence of modifications of a generic map by homotopy moves, is given in [27].

We can now apply our algorithm for Theorem 5.3 to homotope this indefinite fibration to a directed broken Lefschetz fibration with connected fibers and embedded round image, whose round locus realizes Z with its prescribed twisting data (for the local models). This procedure already includes the algorithms for Theorems 4.1 and 4.2 to obtain a directed indefinite fibration with embedded round image, and the ones for Proposition 4.4 to make all the fibers connected. All is achieved by always-realizable moves flip, cusp merge, unsink, push, criss-cross braiding, C-move, $\mathrm{R2}^0$, $\mathrm{R2}^1$, $\mathrm{R2}_2$, $\mathrm{R3}_2$ and $\mathrm{R3}_3$. □

As a corollary, we obtain a purely topological and algorithmic construction —from any given generic map— of *simplified broken Lefschetz fibrations* introduced in [6], as well as that of *simplified wrinkled fibrations* introduced in [79] on arbitrary closed 4–manifolds. (These are simplified indefinite fibrations without cusps and without Lefschetz singularities, respectively.)

[2] In [70], surgery moves were used algorithmically, while in [71], another definite fold elimination technique is introduced without involving such surgery moves. In the latter, for example, a sequence of moves as depicted in Figure 43 is used.

Corollary 6.2. *There is an explicit algorithm, consisting of always-realizable base diagram moves, which turns any generic map from a closed oriented 4–manifold X to S^2 to a simplified broken Lefschetz fibration (or to a simplified wrinkled fibration). Therefore, any closed oriented connected 4–manifold X admits a simplified broken Lefschetz fibration.*

Proof. The algorithm for a simplified broken Lefschetz fibration on X is provided by Theorem 6.1 by taking Z as *any* null-homologous circle in X, e.g. a null-homotopic one. Note that the twisting type of Z, since it has only one component, is already governed by the topology of X by Proposition 5.2. We can also turn a simplified broken Lefschetz fibration to a simplified wrinkled fibration [79]: perform flip-and-slips on the round image, but without unsinking the cusps at the end, perturb each Lefschetz singularity using the wrinkling move, and cusp merge all the components (using arcs that project to embedded ones under the fibration map) to one. □

Remark 6.3. The "simplified" term for an indefinite fibration includes all kinds of simplifications we have considered: directed, embedded round image, fiber-connected, connected round image (and all Lefschetz singularities on the higher side if it is a broken Lefschetz fibration). A simplified indefinite fibration yields a beautifully simple presentation of the 4–manifold in terms of loops on a surface [6, 79]. These presentations are far from being unique, though, and the reader should be careful when implementing our algorithms. There are choices in many of the always-realizable base diagram moves we employed, such as the cusp merge or the Reidemeister II type moves, which will result in different presentations on the same surface. (See, e.g., [35, 14].)

Remark 6.4. As we discussed in the Introduction, these are the first purely topological and explicit constructions of broken Lefschetz fibrations on arbitrary 4–manifolds with embedded round images. Earlier handlebody proofs [24, 55, 5, 2], which start with an arbitrary Morse function (similar to our initial generic function), would break the 4–manifold X into two 2–handlebodies X_i, $i = 1, 2$, equip them with broken Lefschetz fibrations with open book boundaries, and match the latter implicitly by invoking powerful results of Eliashberg and Giroux from contact geometry [20, 29]. One exception is the particular case of *doubles*, i.e. when $X_2 = -X_1$, where the open books readily match [24, 42]. These however constitute a rather small class of 4–manifolds.

Next, we provide a construction of broken Lefschetz pencils on near-symplectic 4–manifolds [4, 5, 6].

Theorem 6.5. *Let ω be a near-symplectic form on a closed oriented 4–manifold X with non-empty Z_ω. Then, there exists a fiber-connected directed broken Lefschetz pencil f on X with embedded round image, whose round locus Z_f coincides with Z_ω with the same twisting data, and so that $\omega([F]) > 0$ for any fiber F of f. Given any generic map from $X \setminus B$ to S^2, which has a regular fiber Poincaré dual to an integral near-symplectic form ω, and is a projectivization (i.e. conforming to the local model $(z_1, z_2) \mapsto z_1/z_2$) around each point in a discrete set B of cardinality $[\omega]^2$ in X, such f can be derived from it by an explicit algorithm.*

Generic maps, which satisfy the conditions listed in the last sentence so as to be prototypes for pencils, are found in abundance, as we will demonstrate below. Our proof is an improved version of the proof given in [5].

Proof of Theorem 6.5. We can assume that ω is integral: if needed, approximate ω by a rational near-symplectic form with the same zero locus (and twisting data), and take a positive multiple of it. Let F be a closed oriented surface representing its Poincaré dual. Since $\omega^2 > 0$, we have $[F]^2 = m > 0$, for some integer m. Let $\tilde{X}$ be the blow-up of X at m points on F

and in the complement of Z_ω, $E_1, E_2, \dots, E_m$ the exceptional spheres, and $\tilde{F}$ the proper transform of F. So $[\tilde{F}]^2 = 0$ and each E_j intersects $\tilde{F}$ positively and transversely at one point.

Let N_j be disjoint tubular neighborhoods of E_j, for $j = 1, 2, \dots, m$, and N_0 be a tubular neighborhood of $\tilde{F}$ in $\tilde{X}$. Set $h_0 \colon N_0 \to D^2$ to be the projection onto the D^2–factor of the trivialization $N_0 \cong D^2 \times \tilde{F}$, where the target D^2 is embedded as the southern hemisphere of S^2, and $h_j : N_j \to S^2$ to be the radial projection onto $E_j \cong S^2$. We arrange the latter so that all the D^2–sections of $E_j \cap N_0$ are mapped onto the southern hemisphere of S^2 and that h_j coincides with h_0 on $N_0 \cap N_j$, $1 \le j \le m$. We can now define a surjective map h_N from $N = \bigcup_{j=0}^m N_j$ onto S^2. Here, the preimages of the points of the southern hemisphere are diffeomorphic to $\tilde{F}$, and the preimages of the interior points of the northern hemisphere consist of m copies of 2–disks.

Extend h_N to a continuous map $h \colon \tilde{X} \to S^2$, e.g. by first defining the map on a collar of $\partial(X \setminus \operatorname{Int} N)$ using $h|_{\partial N}$, and then mapping all remaining points in the interior to the northern hemisphere of S^2, which is possible, since the northern hemisphere is contractible. Then approximate this h by a generic map relative to N. Note that h was already a submersion on $\operatorname{Int} N$.

Given such a generic map h, we apply the same algorithm in the proof of Theorem 6.1 to obtain a fiber-connected, directed broken Lefschetz fibration $\tilde{f} \colon \tilde{X} \to S^2$ with embedded round image, whose round locus $Z_{\tilde{f}}$ realizes the given $Z = Z_\omega$ with prescribed local models. Here, Z_ω is identified with its image under the natural inclusion of X minus the blown-up points into $\tilde{X}$, with the same local data. Performing all the modifications away from $N' = \bigcup_{j=1}^m N_j$, we can guarantee that $\tilde{f}|_{N'} = h|_{N'}$. (This is possible, since $\tilde{f}$ is a submersion on $\partial(X \setminus \operatorname{Int} N')$; see Remark 4.5. For the elimination process of definite folds, the procedures given in [5, 70] work the same in the case of a manifold with boundary.) Moreover, we can still assume that $\tilde{f}$ is a submersion over the southern hemisphere, but with fibers that possibly have different genera than the original $\tilde{F}$. (Because some of our procedures might use base diagram moves that swing a fold arc over this region.) Every fiber of $\tilde{f}$, which are all homologous to the original $\tilde{F}$ even if $\tilde{F}$ is no longer a fiber, intersects each E_j positively and transversely at one point. So, each exceptional sphere E_j is a section of this broken Lefschetz fibration, and blowing-down all we obtain the desired pencil. □

This provides an alternate, purely topological and constructive proof of the harder direction of the main result, Theorem 1, of [4], together with some of its enforcements, such as having a pencil with directed and embedded round image. The authors' proof in [4] instead used approximately holomorphic techniques of Donaldson to establish the existence of these broken Lefschetz pencils implicitly.

We fall short of capturing another enforcement in [4] that seems out of reach for "softer" techniques: making the fibers symplectic with respect to the given near-symplectic form away from its zero locus. Nevertheless, the converse result of [4], which is a Thurston–Gompf type construction of a near-symplectic form on a given broken Lefschetz pencil (for which the fibers are symplectic, called a *near-symplectic pencil*), allows us to reproduce the following result of [6] without appealing to approximately holomorphic techniques.

Corollary 6.6. *Any closed oriented connected 4–manifold X with $b_2^+(X) > 0$ admits a near-symplectic simplified broken Lefschetz pencil.*

Proof. Since $b_2^+(X) > 0$, there is a closed oriented surface F in X with $F^2 > 0$. We can run the same procedure in the proof of Theorem 6.5 with this F and *any* (non-empty) null-homologous connected 1–manifold Z in X. (Once again, the twisting data is governed by

the topology of X.) The result is a simplified broken Lefschetz pencil f on X. Fibers are all homologous to F, which has positive square. Using the cohomology class which is the Poincaré dual of $[F]$, we can employ the Thurston–Gompf type construction of [4, Proof of Theorem 3] to build a near-symplectic form ω on X, with respect to which all fibers of f are symplectic away from the singular locus. □

7. Constructions of simplified trisections of 4–manifolds

In this last section, we give algorithmic constructions of trisections of 4–manifolds, which will utilize homotopy modifications of generic maps discussed in earlier sections. Our first goal is to describe a correspondence between broken Lefschetz fibrations and trisections of 4–manifolds. Meanwhile, we will prove that one can derive a rather special Gay–Kirby trisection of any 4–manifold from a given broken Lefschetz fibration on it, which we will call a *simplified trisection*. We will then move on to presenting various new constructions of (simplified) trisections of 4–manifolds using this dictionary.

7.1. **Broken Lefschetz fibrations to trisections and back.**

We begin with discussing how to derive a trisection from a broken Lefschetz fibration. Since we already have procedures to homotope any given broken Lefschetz fibration to a simplified (or a bit more generally, fiber-connected, directed) broken Lefschetz fibration, we will content ourselves with presenting our arguments for such broken Lefschetz fibrations. As in the original proof of Gay and Kirby in [28], the trisection we obtain will be induced by a certain generic map (trisected Morse 2–function) to the 2–sphere. However, the trisections we get will be rather special: they do not have *any* non-trivial "Cerf boxes" (where handle slides occur due to crossings between indefinite fold circles) and cusps only appear in triples (on the same singular circle). See Figure 42 below. Following our earlier terminology, we call such a trisection a *simplified trisection*. From such a generic map, one can obtain a trisection decomposition by looking at the three sectors shown in Figure 42 (b), in the same way as argued in [28].

Theorem 7.1 (Broken Lefschetz fibrations to trisections)**.** *Let X admit a fiber-connected, directed broken Lefschetz fibration $f\colon X \to S^2$ with embedded round image. Let f have $k \geq 0$ Lefschetz singularities, $\ell \geq 0$ round locus components, and lowest regular fiber genus g. Then there exists a simplified (g', k')–trisection of X, with $(g', k') = (2g + k + \ell + 2, 2g + \ell)$.*

Proof. Note that the broken Lefschetz fibration $f\colon X \to S^2$ as in the theorem is of genus $g+\ell$. The *genus* of such a broken Lefschetz fibration here is defined as that of a generic fiber with the highest genus. Consider the decomposition $S^2 \cong D^2_+ \cup (S^1 \times [-1,1]) \cup D^2_-$, where D^2_+ (resp. D^2_-) is contained in the interior of the northern (resp. southern) hemisphere, $S^1 \times \{0\}$ corresponds to the equator, $S^1 \times [-1,1]$ is a regular neighborhood of the equator, and the three pieces are glued along their boundaries. We may assume that all the Lefschetz critical values and the round image are contained in $\operatorname{Int} D^2_+$ in such a way that the round image is outward-directed in D^2_+. Then, we have a trivialization $\rho\colon f^{-1}(S^1 \times [-1,1]) \to S^1 \times [-1,1] \times \Sigma_g$, where the restriction of f is the composition of ρ with the projection $S^1 \times [-1,1] \times \Sigma_g \to S^1 \times [-1,1]$. We will show how to "fold" the fibration f along this region to get a new generic map with a definite fold, and then simplify it to obtain the desired generic map yielding a trisection.

Let $h : \Sigma_g \to [1,2]$ be a standard Morse function with exactly $2g$ index–1 critical points, one index–0 critical point, x_1, and one index–2 critical point, x_2, for which $h(x_1) = 1$ and $h(x_2) = 2$. Define the smooth function $\varphi\colon [-1,1] \times \Sigma_g \to [1,3]$ by $\varphi(t,x) = h(x)\cos(\pi t/2)+1$, $(t,x) \in [-1,1] \times \Sigma_g$ (see Figure 40). We can easily check that φ is a Morse function with $\varphi^{-1}(1) = \{-1,1\} \times \Sigma_g$ and that its critical points $\operatorname{Crit}(\varphi)$ coincide with those of h on $\{0\} \times \Sigma_g$:

i.e. we have $\mathrm{Crit}(\varphi) = \{0\} \times \mathrm{Crit}(h)$. Furthermore, a critical point of index λ for h corresponds to a critical point of index $\lambda + 1$ for φ.

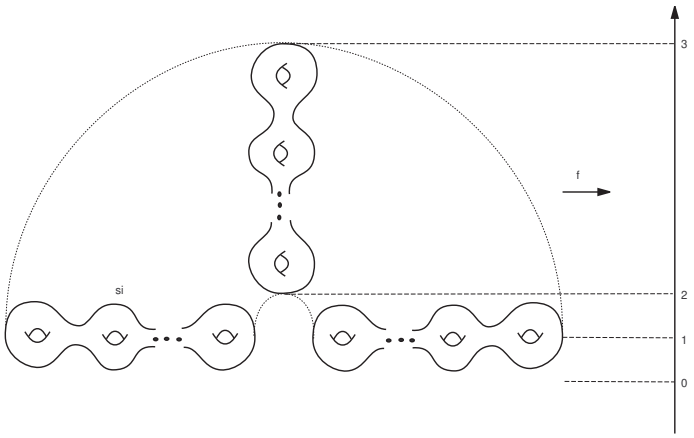

FIGURE 40. Morse function φ.

Let $\pi_\pm \colon D^2_\pm \to \mathbb{R}^2$ be the standard projections $S^2 \to \mathbb{R}^2$ of the unit 2–sphere restricted to $D^2_\pm$ composed with an appropriate multiplication by a positive constant so that their image coincides with the unit disk in $\mathbb{R}^2$. Define the smooth map $g_0 \colon X \to \mathbb{R}^2$ by $g_0|_{f^{-1}(D^2_\pm)} = \pi_\pm \circ f$ and $g_0|_{f^{-1}(S^1 \times [-1,1])} = \eta \circ (\mathrm{id}_{S^1} \times \varphi) \circ \rho$, where $\eta \colon S^1 \times [1,3] \hookrightarrow \mathbb{R}^2$ is an appropriate embedding.

Then, g_0 has folds and Lefschetz singularities and its fold image consists of concentric circles. The innermost ones correspond to the original round image R_0 and are outward-directed. Then comes an inward-directed circle, and the others are outward-directed except the outermost one which is a definite fold image (see the top-left of Figure 41). Using $\mathrm{R2}^0$ and $\mathrm{R2}_2$ moves we can change the order of R_0 and the inward-directed circle, so now only the innermost circle is inward-directed. This, too can be reverted using flip and slip and push moves. However, unlike earlier, here we only unsink *one* of the 4 cusp points on the reverted circle. Now the round image is directed outwards; the innermost circle has 3 cusps, and all the Lefschetz critical values (including one new point) are in the central region (see Figure 41).

We can now wrinkle one of the Lefschetz singularities to get a "triangle"; an indefinite fold circle with exactly 3 cusps as in Figure 4, whose image is embedded and directed outwards. Push all the other Lefschetz singularities into this triangle, and repeat the same procedure until no Lefschetz singularity is left. We finally get a generic map $g \colon X \to \mathbb{R}^2$, which has directed, embedded round image, with an embedded definite fold image as its outermost circle; see Figure 42 (b). The innermost $k+2$ circles all have 3 cusps, where k is the number of Lefschetz critical points of the original broken Lefschetz fibration $f \colon X \to S^2$. The remaining $2g + \ell$ indefinite circles contain no cusps.

The map $g \colon X \to \mathbb{R}^2$ prescribes a $(2g + k + \ell + 2, 2g + \ell)$–trisection of X. (As in [28], this map yields a trisection decomposition of X by looking at the three sectors shown in Figure 42 (b).) □

Remark 7.2 (Trisections from –simplified broken– Lefschetz fibrations). For a genus–$(g+1)$ *simplified* broken Lefschetz fibration $f \colon X \to S^2$ with non-empty round locus and k Lefschetz singularities, we get a $(2g + k + 3, 2g + 1)$–trisection on X. For an honest genus–g Lefschetz

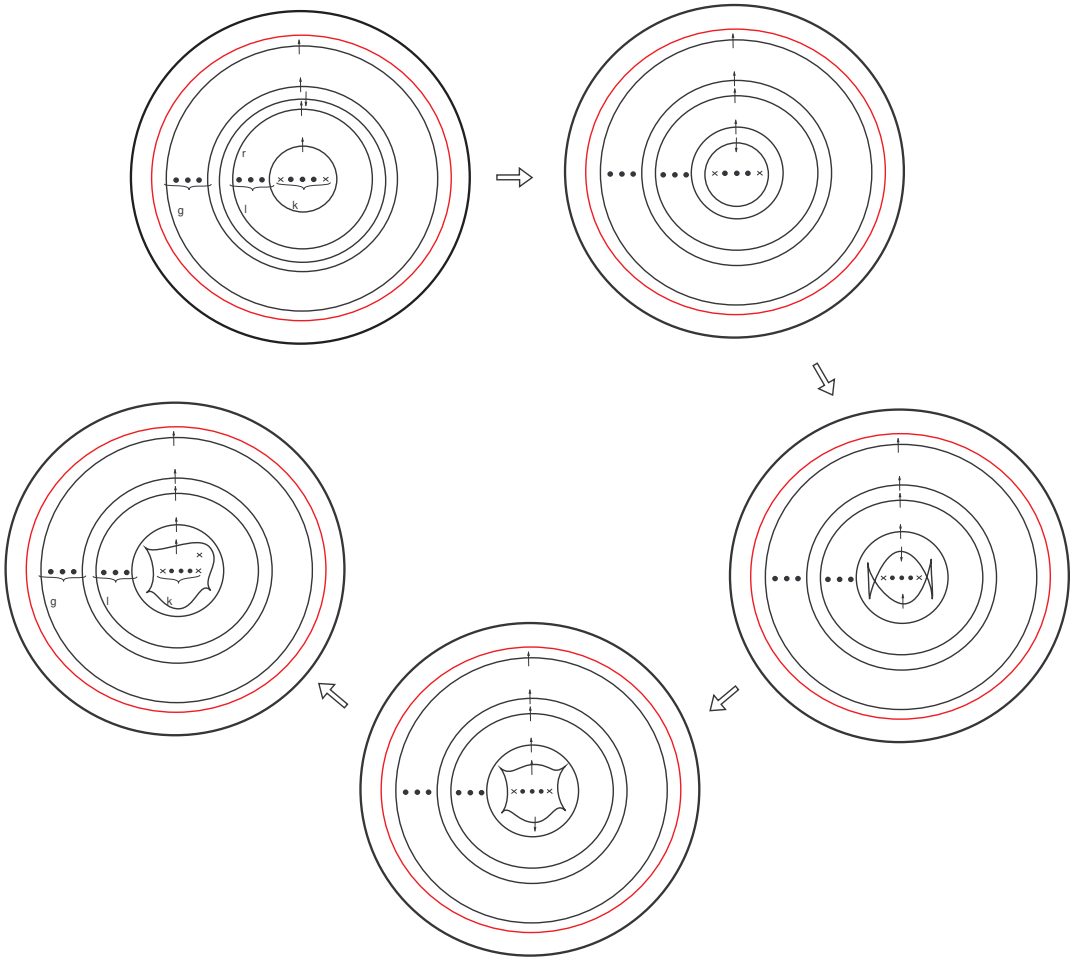

FIGURE 41. The round image of g_0 embedded in $D^2_+ \cup (S^1 \times [-1,1]) \cong D^2$, where the red circle represents a definite fold image. Then, we arrange it using $\mathrm{R2}^0$, $\mathrm{R2}_2$, push and unsink moves.

fibration, we get a $(2g+k+2, 2g)$–trisection. One can also allow f to have *achiral* Lefschetz singularities, where we also accept local orientation-preserving models $(z_1, z_2) \mapsto z_1\bar{z}_2$ around singular points. The *base diagram* of the trisection map itself will be insensitive to achirality.

Our construction of trisections from Lefschetz fibrations can be seen to be complementary to Gay's work in [23], where he produces trisections from Lefschetz *pencils*, which *always have base points*. That is a very different construction, and the author points out that it does *not* work for Lefschetz fibrations [23, Remark 7]. Another construction via trisection diagrams for Lefschetz pencils with one base point was recently given in [18].

Remark 7.3. It should be clear from our proof that we can also derive a Gay–Kirby trisection by "folding" any fiber-connected, directed broken Lefschetz fibration, which does not necessarily have an embedded image. Though in this case, the resulting trisection will not be simplified either.

Together with Corollary 6.2 from the previous section, the construction in Theorem 7.1 establishes the existence of simplified trisections on arbitrary 4–manifolds.

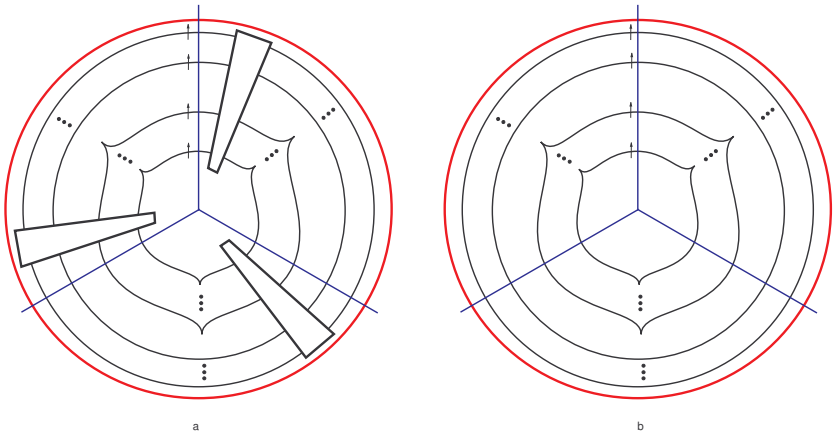

FIGURE 42. (a) Singular image of general Gay–Kirby trisections with Cerf boxes; (b) simplified Gay–Kirby trisections we produce.

Corollary 7.4 (Existence of simplified trisections)**.** *Any closed connected oriented* 4*–manifold* X *admits a simplified trisection, and such a trisection can be constructed algorithmically from any given generic map from* X *to* S^2*.*

Remark 7.5 (Handle slides in simplified trisections and their diagrams). The main difference between a general trisection and a simplified one is in the *hierarchy of handle slides*, which is imposed by the special structure of the simplified trisections. If we take any radial cut of the base disk from the center to its boundary, while avoiding the cusp points, the inverse image of this ray is a genus–g handlebody, given by g disjoint embedded simple closed curves $\{\alpha_1, \alpha_2, \dots, \alpha_g\}$ on a central reference fiber $F \cong \Sigma_g$. Each α_i comes from the fiberwise 2–handle attachment prescribed by the corresponding $(g+1-i)$–th indefinite fold arc image the ray crosses over, for $i = 1, 2, \dots, g$. In a general trisection, moving across a *non-trivial* Cerf box, these 2–handles prescribed by α_i can slide over each other in any fashion. In particular, the roles of any two α_i and α_j with $i \neq j$ might be interchanged. In a simplified trisection however, the 2–handle corresponding to an α_i slides over that corresponding to α_j only if $i < j$. That is, these handle slides only occur in an "upper-triangular fashion" in simplified trisections.

Recall that trisection decompositions of 4–manifolds can also be described by *trisection diagrams*: collections of g disjoint curves $\{\alpha_i\}, \{\beta_i\}, \{\gamma_i\}$ on Σ_g, which pairwise give Heegaard diagrams for connected sums of copies of $S^1 \times S^2$ [28]. In a general trisection, the curves $\{\alpha_i\}$, $\{\beta_i\}$, $\{\gamma_i\}$ of a corresponding trisection diagram can be pairwise made into a standard Heegaard diagram for connected sums of copies of $S^1 \times S^2$ after various handle slides among the same collection of curves (and a self-diffeomorphism of Σ_g), whereas in a simplified trisection, once again, it suffices to perform handle slides in an "upper-triangular fashion", e.g. only sliding α_i over α_j for $i < j$. Hayano's recent work on diagrams of simplified trisections [36] provides yet another characterization akin to the monodromy characterization for simplified broken Lefschetz fibrations [6, 9] —whereas such a characterization does not exist for general trisections or broken Lefschetz fibrations.

We also have the converse result:

Proposition 7.6 (Trisections to broken Lefschetz fibrations)**.** *Let* X *admit a* (g', k')*–trisection. Then there exists a fiber-connected, directed broken Lefschetz fibration* $f\colon X \to S^2$*, which has regular fibers of highest genus* g *and with* k *Lefschetz singularities, where* $g = g' + 2$ *and*

$k = 3g' - 3k' + 4$. *If the given trisection is simplified, then f in addition has embedded round image.*

Proof. By embedding $\mathbb{R}^2$ into S^2 in such a way that the central region contains the north pole, we consider the generic map given by the trisection as a map into S^2. We then use a version of flip and slip for the definite fold, which first appeared in [79] (where the author attributes the idea to Gay) and later in [25, Fig 7]. Note that here the arrows on definite folds indicate the fiberwise index–3 handle attachment direction. This modification is depicted by a series of base diagram moves in Figure 43. By arguments identical to those we have for the indefinite case, the versions of flips and unflips involving definite folds here are always-realizable, and so are the Reidemeister type $\mathrm{R2}_2$ moves. Now the image of the definite fold circle turns into that of an indefinite fold circle which is directed towards the image of the original map.

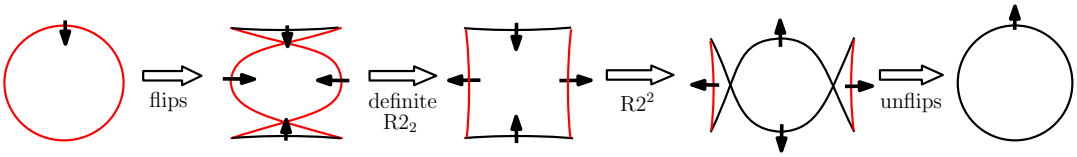

FIGURE 43. Turning a definite fold circle to an indefinite one. Red lines depict definite fold images, while black lines depict indefinite fold images.

By always-realizable $\mathrm{R2}^0$, $\mathrm{R2}_2$, $\mathrm{R3}_3$ and C–moves, we can move the new indefinite circle to the north pole. We then apply flip and slip to it around the north pole. Unsink all the cusps and push them to the innermost region of this fiber-connected, directed broken Lefschetz fibration. The genus of a regular fiber in the innermost circle is now $g = g' + 2$, and we get exactly $k = 3(g' - k') + 4$ Lefschetz critical points. □

Remark 7.7. The original proof of Gay–Kirby for the existence of trisections on arbitrary 4–manifolds in [28] also goes through –a rather different– explicit sequence of homotopy modifications of generic maps. Given an arbitrary Gay–Kirby (g', k')–trisection, we can apply Proposition 7.6 and Theorem 4.2 to eliminate the non-trivial Cerf boxes. Then applying Theorem 7.1, we get back a simplified (g'', k'')–trisection —typically with *genus* g'' higher than the original genus g'.

Remark 7.8 (Stable uniqueness for simplified trisection decompositions). Gay and Kirby's stable uniqueness of trisection decompositions on a 4–manifold holds within the subclass of simplified trisection decompositions (i.e. the decompositions induced by simplified trisection maps we have built) . This follows from the following line of arguments: In the next subsection we construct a simplified $(3, 1)$–trisection on S^4. By the work of Hayano in [36], this has a trisection diagram that can be seen to be handle slide equivalent to a trisection diagram for the standard $(3, 1)$–trisection used by Gay and Kirby in their stabilization result. One can thus use our simplified trisection on S^4 instead to arrive at the same conclusion. Each time we stabilize a simplified (g', k')–trisection on a 4–manifold using the simplified $(3, 1)$–trisection, the connected sum model yields a new $(g' + 3, k' + 1)$–trisection, where the 3 innermost circles consist of an indefinite fold C with no cusps and two other triple-cusped ones enclosed by it —all coming from the $(3, 1)$–trisection on S^4. Since the attaching circles of the original (g', k')–trisection and the additional $(3, 1)$–piece are independent, one can not only apply the always-realizable $\mathrm{R2}^1$ moves, but in this case $\mathrm{R2}_1$ moves (compare with Remark 3.5) and their analogues for crossing over cusps as well so as to "expand" C all the way across the triple-cusped folds coming from the original (g', k')–trisection. This guarantees that the resulting

trisection has the same nested picture, where the cusps only appear in the inner-most circles. This argument shows that the stabilization of a simplified trisection decomposition is again simplified as trisection decomposition.

7.2. **Exotic trisections.**

The list of 4–manifolds that admit $g' = 0$, 1, or 2 trisections is very short: the only $g' = 0$ trisection is for S^4 and $g' = 1$ examples are for $\mathbb{CP}^2$, $\overline{\mathbb{CP}}^2$ and $S^1 \times S^3$ [28], whereas a $g' = 2$ trisection is either a connected sum of these $g' = 1$ examples or is a trisection of $S^2 \times S^2$ [60]. Thus Meier and Zupan posed the following natural question [60, Question 1.2]: *What is the smallest value of g' for which there are infinitely many 4–manifolds which admit (g', k')–trisection for some k'?*

Theorem 7.1, combined with earlier constructions of simplified broken Lefschetz fibrations, addresses this question (and provides an alternate to the answer given in [61]):

Corollary 7.9. *For every fixed $g' \geq 3$ and $g'-2 \geq k' \geq 1$, there are infinitely many homotopy inequivalent 4–manifolds admitting (g', k')–trisections.*

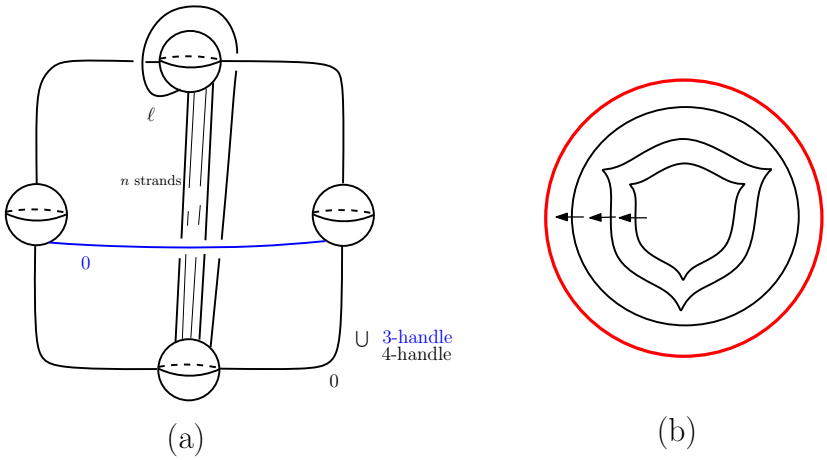

FIGURE 44. (a) Kirby diagram for genus–1 simplified broken Lefschetz fibrations on rational homology 4–spheres L_n and L'_n, for ℓ even and odd, respectively. The 2–handle and the 3–handle that make up the round 2–handle are given in blue. For $n = 1$ we have S^4. (b) The base diagram for a simplified trisection on L_n and L'_n we obtain from these simplified broken Lefschetz fibrations.

Proof. As shown in [10, 33], an infinite family of homotopy inequivalent 4–manifolds, namely the rational homology 4–spheres L_n and L'_n (say for $n \geq 2$), admit genus–1 simplified broken Lefschetz fibrations with no Lefschetz singularities. A handlebody description of these simplified broken Lefschetz fibrations (following [6]) is given in Figure 44 (a). It is easy to see that $H_1(L_n; \mathbb{Z}) = H_1(L'_n; \mathbb{Z}) = \mathbb{Z}_n$ for $n \geq 2$.

By Theorem 7.1, these yield simplified $(3, 1)$–trisections; see Figure 44 (b) for the base diagram. We can use connected sums with standard trisections [28] (e.g. with standard $(1, 0)$ and $(1, 1)$ trisections on $\overline{\mathbb{CP}}^2$ and $S^1 \times S^3$, respectively) to arrive at the other higher (g', k') examples in the statement. □

Example 7.10. An interesting example is the simplified $(3,1)$–trisection we derive from the genus–1 simplified broken Lefschetz fibration on S^4 [4]. The Morse 2–function for this trisection we get has 2 indefinite circles with 3 cusps on each, and one outer indefinite circle with no cusps; see Figure 44 for its base diagram. (The $(3,1)$–trisections of infinitely many rational homology spheres we obtained in the proof of Corollary 7.9 all have the same base diagram.) On the other hand, the "standard trisection" of S^4 [28, Figure 27] used for stabilization comes from a Morse 2–function with 3 indefinite circles with 2 cusps on each. After three C–moves, one can obtain the same base diagrams outside of the Cerf boxes.

Remark 7.11. Shortly after publicizing our article, Meier gave another nice construction of $(3,1)$–trisections on twist spun 3–manifolds [58], by also employing some allowable base diagram moves. It would be interesting to compare these examples, since, akin to the classification of low genera simplified broken Lefschetz fibrations [33, 10], one might expect the list of (simplified) $(3,1)$–trisections to consist of fairly standard ones.

A natural idea for relating newly emerging theory of trisections of 4–manifolds to constructions of exotic smooth structures is to find (g',k')–trisections, whose three sectors can be re-glued in a way the diffeomorphism type is changed, but the homeomorphism type remains the same. Perhaps what is more interesting than the above question is to find the smallest g' for which there are infinitely many non-diffeomorphic 4–manifolds *in the same homeomorphism class* admitting a (g',k')–trisection, for some k' —what one can call (small) *exotic trisections*. We finish with presenting some examples:

Corollary 7.12. *There is an infinite family of exotic* $(34,8)$*–trisections in the homeomorphism class of* $\mathbb{CP}^2\#9\overline{\mathbb{CP}}^2$*. There is an exotic* $(20,4)$*–trisection in the homeomorphism class of* $\mathbb{CP}^2\#7\overline{\mathbb{CP}}^2$*.*

Proof. As shown by Fintushel and Stern, a knot surgered elliptic surface $E(1)_K$ admits a genus–$2h$ Lefschetz fibration, for K a genus–h fibered knot [22]. For a family of genus–2 fibered knots K_i with distinct Alexander polynomials, we obtain a family of genus–4 Lefschetz fibrations (X_i,f_i), where X_i are mutually non-diffeomorphic irreducible symplectic 4–manifolds all in the same homeomorphism class. Per Remark 7.2, we derive an infinite family of exotic $(34,8)$–trisections from these examples. Standard $E(1)=\mathbb{CP}^2\#9\overline{\mathbb{CP}}^2$ also admits a $(34,8)$–trisection: Applying our procedure to the elliptic Lefschetz fibration on $E(1)$ (where $g=1$, $k=12$), we obtain a $(16,2)$–trisection, which we can then stabilize 6 times (with a $(3,1)$–trisection on S^4) to get a $(34,8)$–trisection on $E(1)$ as well.

For a smaller (but a single) example, we can take the genus–2 Lefschetz fibration on an exotic, irreducible symplectic $\mathbb{CP}^2\#7\overline{\mathbb{CP}}^2$ constructed in [11], and apply Theorem 7.1 to produce a $(20,4)$–trisection. The standard $\mathbb{CP}^2\#7\overline{\mathbb{CP}}^2$ also admits a $(20,4)$–trisection: Take a rational Lefschetz fibration on it with 6 singular points, apply our procedure, and then stabilize it 4 times. □

Remark 7.13. Per the very nature of our article, we have only discussed trisections as a certain class of generic maps in this article. It would be interesting to analyze our examples, especially the exotic pairs (or other such examples that appeared later in [54]), in terms of induced trisection diagrams, which can be derived following the explicit procedures given in [17, 16].

References

[1] A. Abrams, D. Gay and R. Kirby, "Group trisections and smooth 4–manifolds", Geom. Topol. **22** (2018), no. 3, 1537–1545.

[2] S. Akbulut and C. Karakurt, ‘‘Every 4–manifold is BLF”, J. Gökova Geom. Topol. GGT **2** (2008) 83–106.
[3] Y. Ando, ‘‘Elimination of certain Thom–Boardman singularities of order two”, J. Math. Soc. Japan **34** (1982), no. 2, 241–267.
[4] D. Auroux, S. Donaldson, and L. Katzarkov, ‘‘Singular Lefschetz pencils”, Geom. Topol. **9** (2005), 1043–1114.
[5] R.I. Baykur, ‘‘Existence of broken Lefschetz fibrations”, Int. Math. Res. Not. IMRN (2008), Art. ID rnn 101, 15 pp.
[6] R.I. Baykur, ‘‘Topology of broken Lefschetz fibrations and near-symplectic 4–manifolds”, Pacific J. Math. **240** (2009), no. 2, 201–230.
[7] R.I. Baykur, ‘‘Handlebody argument for modifying achiral singularities”, appendix to [55], Geom. Topol. **13** (2009), 312–317.
[8] R.I. Baykur, ‘‘Broken Lefschetz fibrations and smooth structures on 4–manifolds”, Proceedings of the Freedman Fest, pp. 9–34, Geom. Topol. Monogr., Vol. 18, Geom. Topol. Publ., Coventry, 2012.
[9] R.I. Baykur and K. Hayano, ‘‘Broken Lefschetz fibrations and mapping class groups”, Geom. Topol. Monogr., Vol. 19 (2015), 269–290.
[10] R.I. Baykur and S. Kamada, ‘‘Classification of broken Lefschetz fibrations with small fiber genera”, J. Math. Soc. Japan **67** (2015), 877–901.
[11] R.I. Baykur and M. Korkmaz, ‘‘Small Lefschetz fibrations and exotic 4–manifolds”, Math. Ann. **367** (2017), 1333–1361.
[12] R.I. Baykur and O. Saeki, ‘‘Simplified broken Lefschetz fibrations and trisections of 4–manifolds”, Proc. Natl. Acad. Sci. USA **115** (2018), 10894–10900.
[13] S. Behrens, ‘‘On 4–manifolds, folds and cusps”, Pacific J. Math. **264** (2013), 257–306.
[14] S. Behrens and K. Hayano, ‘‘Elimination of cusps in dimension 4 and its applications”, Proc. London Math. Soc. **113** (2016), 674–724.
[15] E.H. Brown, Jr., ‘‘The cohomology of BSO_n and BO_n with integer coefficients”, Proc. Amer. Math. Soc. **85** (1982), 283–288.
[16] N.A. Castro, ‘‘Trisecting smooth 4–dimensional cobordisms”, preprint; arxiv.org/abs/1703.05846.
[17] N.A. Castro, D. Gay and J. Pinzón-Caicedo, ‘‘Diagrams for relative trisections”, Pacific J. Math. **294** (2018), 275–305.
[18] N.A. Castro and B. Ozbagci, ‘‘Trisections of 4–manifolds via Lefschetz fibrations”, Mathematical Research Letters **26** (2019), 383–420.
[19] F. Costantino and D. Thurston, ‘‘3-manifolds efficiently bound 4-manifolds”, J. Topol. **1** (2008), 703–745.
[20] Y. Eliashberg, ‘‘Classification of overtwisted contact structures on 3–manifolds”, Invent. Math. **98** (1989), 623–637.
[21] Y. Eliashberg and N. M. Mishachev, ‘‘Wrinkling of smooth mappings and its applications. I”, Invent. Math. **130** (1997), 345–369.
[22] R. Fintushel and R. Stern, ‘‘Families of simply connected 4–manifolds with the same Seiberg–Witten invariants”, Topology **43** (2004), no. 6, 1449–1467.
[23] D. Gay, ‘‘Trisections of Lefschetz pencils”, Algebr. Geom. Topol. **16** (2016), 3523–3531.
[24] D. Gay and R. Kirby, ‘‘Constructing Lefschetz-type fibrations on four-manifolds”, Geom. Topol. **11** (2007), 2075–2115.
[25] D. Gay and R. Kirby, ‘‘Fiber-connected, indefinite Morse 2–functions on connected n–manifolds”, Proc. Natl. Acad. Sci. USA **108** (2011), 8122–8125.
[26] D. Gay and R. Kirby, ‘‘Reconstructing 4–manifolds from Morse 2–functions”, Proceedings of the Freedman Fest, pp. 103–114, Geom. Topol. Monogr., 18, Geom. Topol. Publ., Coventry, 2012.
[27] D. Gay and R. Kirby, ‘‘Indefinite Morse 2–functions; broken fibrations and generalizations”, Geom. Topol. **19** (2015), 2465–2534.
[28] D. Gay and R. Kirby, ‘‘Trisecting 4–manifolds”, Geom. Topol. **20** (2016), 3097–3132.
[29] E. Giroux, ‘‘Géométrie de contact: de la dimension trois vers les dimensions supérieures”, Proceedings of the International Congress of Mathematicians, Vol. II (Beijing, 2002), Higher Ed. Press, Beijing (2002), 405–414.
[30] M. Gromov, ‘‘Singularities, expanders and topology of maps. I. Homology versus volume in the spaces of cycles”, Geom. Funct. Anal. **19** (2009), 743–841.
[31] J. Hass, A. Thompson and W. Thurston, ‘‘Stabilization of Heegaard splittings”, Geom. Topol. **13** (2009), no. 4, 2029–2050.
[32] A. Hatcher and J. Wagoner, ‘‘Pseudo-isotopies of compact manifolds”, Astérisque, No. 6, Soc. Math. France, Paris, 1973.

[33] K. Hayano, ''On genus-1 simplified broken Lefschetz fibrations", Algebr. Geom. Topol. **11** (2011), 1267–1322.
[34] K. Hayano, ''A note on sections of broken Lefschetz fibrations", Bull. London Math. Soc. **44** (2012), no. 4, 823–836.
[35] K. Hayano, ''Modification rule of monodromies in an R2–move", Algebr. Geom. Topol. **14** (2014), no. 4, 2181–2222.
[36] K. Hayano, ''On diagrams of simplified trisections and mapping class groups", Osaka J. Math. **57** (2020), 17–37.
[37] K. Hayano and M. Sato, ''Four-manifolds admitting hyperelliptic broken Lefschetz fibrations", Michigan Math. J. **62** (2013), no. 2, 323–351.
[38] K. Hayano and M. Sato, ''A signature formula for hyperelliptic broken Lefschetz fibrations", Topology Appl. **173** (2014), 157–174.
[39] F. Hirzebruch and H. Hopf, ''Felder von Flächenelementen in 4–dimensionalen Mannigfaltigkeiten", Math. Ann. **136** (1958), 156–172.
[40] K. Honda, ''Transversality theorems for harmonic forms", Rocky Mountain J. Math. **34** (2004), 629–664.
[41] K. Honda, ''Local properties of self-dual harmonic 2–forms on a 4–manifold", J. Reine Angew. Math. **577** (2004), 105–116.
[42] M.C. Hughes, ''Constructing broken Lefschetz fibrations from handle decompositions", preprint; arxiv.org/abs/1511.08917.
[43] G. Islambouli, ''Comparing 4–manifolds in the pants complex via trisections", Algebr. Geom. Topol. **18** (2018), 1799–1822.
[44] G. Islambouli, ''Nielsen equivalence and trisections of 4–manifolds", preprint; https://arxiv.org/abs/1804.06978.
[45] S. Jabuka and T. Mark, ''Heegaard Floer homology of certain mapping tori", Algebr. Geom. Topol. **4** (2004), 685–719.
[46] S. Jabuka and T. Mark, ''Heegaard Floer homology of certain mapping tori II", Geometry and topology of manifolds, pp. 119–135, Fields Inst. Commun., 47, Amer. Math. Soc., Providence, RI, 2005.
[47] S. Jabuka and T. Mark, ''On the Heegaard Floer homology of a surface times a circle", Adv. Math. **218** (2008), no. 3, 728–761.
[48] S. Jabuka and T. Mark, ''Product formulae for Ozsváth-Szabó 4–manifold invariants", Geom. Topol. **12** (2008), no. 3, 1557–1651.
[49] S. Kim and M. Miller, ''Trisections of surface complements and the Price twist", Algebr. Geom. Topol. **20** (2020) 343–373.
[50] R. Kirby, ''Trisections of 4–manifolds", Proc. Natl. Acad. Sci. USA **115** (2018), 10853–10856.
[51] R. Kirby, P. Melvin and P. Teichner, ''Cohomotopy sets of 4–manifolds", Geom. Topol. Monogr. **18** (2012) 161–190.
[52] P. Lambert-Cole, ''Bridge trisections in $\mathbb{CP}^2$ and the Thom conjecture", to appear in Geom. Topol., preprint; https://arxiv.org/abs/1807.10131.
[53] P. Lambert-Cole, ''Trisections, intersection forms and the Torelli group", Algebr. Geom. Topol. **20** (2020), 1015–1040.
[54] P. Lambert-Cole and J. Meier, ''Bridge trisections in rational surfaces", preprint; https://arxiv.org/abs/1810.10450.
[55] Y. Lekili, ''Wrinkled fibrations on near-symplectic manifolds", Geom. Topol. **13** (2009), 277–318.
[56] H.I. Levine, ''Elimination of cusps", Topology **3**, no. 2 (1965), 263–296.
[57] H.I. Levine, ''Singularities of differentiable mappings", Lecture Notes in Math., Vol. 192, pp. 1–89, Springer, 1971.
[58] J. Meier, ''Trisections and spun four-manifolds", Math. Res. Lett. **25** (2018), no. 5, 1497–1524.
[59] J. Meier, T. Schirmer and A. Zupan, ''Classifying trisections and the Generalized Property R Conjecture", Proc. Amer. Math. Soc. **144** (2016), no. 11, 4983–4997.
[60] J. Meier and A. Zupan, ''Genus-two trisections are standard", Geom. Topol. **21** (2017), no. 3, 1583–1630.
[61] J. Meier and A. Zupan, ''Bridge trisections of knotted surfaces in S^4", Trans. Amer. Math. Soc. **369** (2017), no. 10, 7343–7386.
[62] P. Ozsváth and Z. Szabó, ''Holomorphic triangle invariants and the topology of symplectic four-manifolds", Duke Math. J. **121** (1) (2004), 1–34.
[63] P. Ozsváth and Z. Szabó, ''Holomorphic triangles and invariants for smooth four-manifolds", Adv. Math. **202** (2006), no. 2, 326–400.

[64] T. Perutz, ''Lagrangian matching invariants for fibred four-manifolds: I", Geom. Topol. **11** (2007), 759–828.
[65] T. Perutz, ''Lagrangian matching invariants for fibred four-manifolds: II", Geom. Topol. **12** (2008), no. 3, 1461–1542.
[66] T. Perutz, ''Zero-sets of near-symplectic forms", J. Symplectic Geom. **4** (2006), no. 3, 237–257.
[67] J. H. Rubinstein and S. Tillmann, ''Multisections of piecewise linear manifolds", preprint; arxiv.org/abs/1602.03279.
[68] O. Saeki, ''Constructing generic smooth maps of a manifold into a surface with prescribed singular loci", Ann. Inst. Fourier (Grenoble) **45** (1995), no. 4, 1135–1162.
[69] O. Saeki, ''Simple stable maps of 3-manifolds into surfaces", Topology **35** (1996), 671–698.
[70] O. Saeki, ''Elimination of definite fold", Kyushu J. Math. **60** (2006), 363–382.
[71] O. Saeki, ''Elimination of definite fold II", Kyushu J. Math. **73** (2019), 239–250.
[72] O. Saeki and T. Yamamoto, ''Singular fibers of stable maps and signatures of 4-manifolds", Geom. Topol. **10** (2006), 359–399.
[73] R. Thom, ''Les singularités des applications différentiables", Ann. Inst. Fourier, Grenoble **6** (1955–1956), 43–87.
[74] R. Thom, ''Stabilité structurelle et morphogénèse", Essai d'une théorie générale des modèles, Mathematical Physics Monograph Series, W.A. Benjamin, Inc., Reading, Mass., 1972.
[75] K. Wehrheim and C.T. Woodward, ''Quilted Floer cohomology", Geom. Topol. **14** (2010), no. 2, 833–902.
[76] K. Wehrheim and C.T. Woodward, ''Functoriality for Lagrangian correspondences in Floer theory", Quantum Topol. **1** (2010), no. 2, 129–170.
[77] H. Whitney, ''On the topology of differentiable manifolds", Lectures in Topology, pp. 101–141, University of Michigan Press, Ann Arbor, Mich., 1941.
[78] H. Whitney, ''On singularities of mappings of euclidean spaces. I. Mappings of the plane into the plane", Ann. of Math. (2) **62** (1955), 374–410.
[79] J. Williams, ''The h-principle for broken Lefschetz fibrations", Geom. Topol. **14** (2010), no. 2, 1015–1063.
[80] J. Williams, ''Existence of two-parameter crossings", Geom. Dedicata (2019), https://doi.org/10.1007/s10711-019-00499-1.
[81] T. Yoshida, Y. Kabata and T. Ohmoto, ''Bifurcation of plane-to-plane map-germs with corank two of parabolic type", Theory of singularities of smooth mappings and around it, pp. 239–258, RIMS Kôkyûroku Bessatsu **B55**, Res. Inst. Math. Sci., Kyoto, 2016.

Department of Mathematics and Statistics, University of Massachusetts, Amherst, MA 01003-9305, USA

Email address: baykur@math.umass.edu

Institute of Mathematics for Industry, Kyushu University, Motooka 744, Nishi-ku, Fukuoka 819-0395, Japan

Email address: saeki@imi.kyushu-u.ac.jp